The dynamics and prethermalization of one-dimensional quantum systems probed through the full distributions of quantum noise

2011 New J. Phys. 13 073018

(http://iopscience.iop.org/1367-2630/13/7/073018)

New Journal of Physics
The open-access journal for physics

The dynamics and prethermalization of one-dimensional quantum systems probed through the full distributions of quantum noise

Takuya Kitagawa[1,4], Adilet Imambekov[2], Jörg Schmiedmayer[3] and Eugene Demler[1]

[1] Harvard-MIT Center for Ultracold Atoms, Department of Physics, Harvard University, Cambridge, MA 02138, USA
[2] Department of Physics and Astronomy, Rice University, Houston, TX 77005, USA
[3] Vienna Center for Quantum Science and Technology, Atominstitut, TU-Wien, Stadionallee 2, 1020 Vienna, Austria
E-mail: takuya.kitagawa@gmail.com

New Journal of Physics **13** (2011) 073018 (42pp)
Received 3 May 2011
Published 12 July 2011
Online at http://www.njp.org/
doi:10.1088/1367-2630/13/7/073018

Abstract. Quantum noise correlations have been employed in several areas of physics, including condensed matter, quantum optics and ultracold atoms, to reveal the non-classical states of the systems. To date, such analyses have mostly focused on systems in equilibrium. In this paper, we show that quantum noise is also a useful tool for characterizing and studying the non-equilibrium dynamics of a one-dimensional (1D) system. We consider the Ramsey sequence of 1D, two-component bosons, and obtain simple, analytical expressions for time evolutions of the full distribution functions for this strongly correlated, many-body system. The analysis can also be directly applied to the evolution of interference patterns between two 1D quasi-coindensates created from a single condensate through splitting. Using the tools developed in this paper, we demonstrate that 1D dynamics in these systems exhibits the phenomenon known as 'prethermalization', where the observables of *non-equilibrium*, long-time transient states become indistinguishable from those of thermal *equilibrium* states.

[4] Author to whom any correspondence should be addressed.

Contents

1. Introduction

The probabilistic character of the Schrödinger wavefunctions manifests itself most directly in quantum noise. In many-body systems, shot-to-shot variations of experimental observables contain rich information about the underlying quantum states. Measurements of quantum noise played a crucial role in establishing non-classical states of photons in quantum optics [1], demonstrating quantum correlations and entanglement in electron interferometers [2] and verifying fractional charge of quasi-particles in quantum Hall systems [3–5]. In atomic physics to date, noise experiments have focused on systems in equilibrium. Recent works include the analysis of counting statistics in atom lasers [6], the establishment of the Hanbury–Brown–Twiss effect for both bosons and fermions [7], the analysis of quantum states in optical lattices [8–12], the observation of momentum correlations in Fermi gases with pairing [13] and the investigation of thermal and quantum fluctuations in one-dimensional (1D) and two-dimensional (2D) condensates [14–21].

In this paper, we demonstrate that analysis of quantum noise should also be a powerful tool for analyzing non-equilibrium dynamics of strongly correlated systems. Here we study two equivalent dynamical phenomena: one given by the interaction-induced decoherence dynamics in Ramsey-type interferometer sequences for two-component Bose mixtures in 1D [22] and another given by the evolution of interference patterns of two 1D condensates created through the splitting of a single condensate [23, 24]. We obtain a complete time evolution of the full distribution function of the amplitude of Ramsey fringes or interference patterns. In the case of Ramsey fringes, the average amplitude of Ramsey fringes measures only the average value of the transverse spin component. On the other hand, full distribution functions are determined by higher-order correlation functions of the spins. Hence, full distribution functions contain considerably more information about the time evolution of the system [24–27] and provide a powerful probe of the nature of the quantum dynamics under study. In particular, we use simple expressions of full distribution functions to demonstrate the phenomena of 'prethermalization' in these 1D systems, where observables in non-equilibrium long-time transient states become indistinguishable from those in thermal equilibrium states.

1D systems with continuous symmetries, including superfluids and magnetic systems, have a special place in the family of strongly correlated systems. Quantum and thermal fluctuations are so extreme that long-range order is not possible in equilibrium. Such systems cannot be analyzed using standard mean-field approaches, yet they can be studied through the application of methods specific to 1D such as exact Bethe ansatz solutions [28–39], an effective description using the Tomonaga–Luttinger and sine-Gordon models [40–45] and a numerical analysis using density-matrix renormalization group and matrix product state methods [46]. Such systems are often considered as general paradigms for understanding strongly correlated systems. 1D systems also give rich examples of integrable systems, where due to the existence of an infinite number of conserved quantities, equilibration does not take place [47–49]. Hence the problem we consider in this paper is important for understanding fundamental issues such as the quantum dynamics of strongly correlated systems and equilibration/non-equilibration of many-body systems, as well as for possible applications of spinor condensates in spectroscopy, interferometry and quantum information processing [50–52].

This work was motivated by recent experiments of Widera *et al* [22], who used two hyperfine states of ^{87}Rb atoms confined in 2D arrays of 1D tubes to perform Ramsey-type interferometer sequences. They observed rapid decoherence of Ramsey fringes and the near absence of spin echo. Their results could not be explained within single-mode approximation that assumes a macroscopic Bose condensation into a single orbital state, but they could be understood in terms of the multi-mode Tomonaga–Luttinger-type model. Yet the enhanced decoherence rate and suppression of spin echo do not provide unambiguous evidence for the origin of decoherence. In this paper, we suggest that crucial evidence for the multi-mode dynamics as a source of decoherence should come from the time evolution of full distribution functions of the Ramsey fringe amplitude. Such distribution functions should be accessible in experiments on atom chips [14, 53–56] from the analysis of shot-to-shot fluctuations.

This paper is organized as follows. In section 2, we describe two physically distinct, but mathematically equivalent, dynamics in 1D systems: namely the dynamics of spins in a Ramsey sequence and the dynamics of phase and contrast in interference patterns between two split condensates created from a single condensate. We start by illustrating the basic physics governing the dynamics studied in this paper and give a summary of the central results including

the prediction of prethermalization phenomena. The formal descriptions of the details of the theory for spin dynamics in the Ramsey sequence start from section 3, where we give the Hamiltonian of the 1D system based on the Tomonaga–Luttinger approach. In section 4, we derive the analytical expression for the time evolution of the full distribution function for a simple case in which charge and spin degrees of freedom decouple. This decoupling limit gives a good approximation to the experimental situation of Widera *et al* [22]. A summary of the result in this decoupling limit has already been given in [52]. A more general case in which spin and charge degrees of freedom mix is studied in section 5. Such mixing introduces the dependence of spin distribution functions on the initial temperature of the system. All the results obtained in sections 4 and 5 can be extended to the study of the dynamics of interference patterns, using the mapping described in section 2. We describe the details of such dynamics of interference patterns for split condensates in section 6. We demonstrate the prethermalization phenomena and show that the interference contrasts of split condensates in a steady state have distributions indistinguishable from those of thermal condensates at some effective temperature $T_{\rm eff}$. We conclude the paper in section 7 with a discussion of possible extensions of this work.

2. A description of one-dimensional (1D) dynamics and a summary of results

2.1. Ramsey dynamics

In this paper, we study the dynamics of 1D, interacting two-component Bose mixtures in the Ramsey-type sequence. In analogy with spin-1/2 particles, we refer to one component as spin-up and the other component as spin-down. In the experiment on cold atoms in [22], two hyperfine states are used for these two components. In the following, we consider a generic situation where there is no symmetry that relates spin-up and spin-down. In particular, unlike fermions with spin-1/2, there is no SU(2) symmetry. In a typical experimental setup with cold atoms, there is a harmonic confinement potential along the longitudinal direction of condensates, but here we assume the absence of such a harmonic trap potential. Our consideration gives a good approximation for the central region of cold atom experiments in the presence of such potentials.

The Ramsey-type sequence is described as follows (figure 1):

1. All atoms are prepared in the spin-up state at low temperature.
2. A $\pi/2$ pulse is applied to rotate the spin of each atom into the x-direction.
3. Spins evolve for time t.
4. Spins in the transverse direction (x–y-plane) are measured.

In a typical experimental situation [22], the last measurement step is done by applying a $\pi/2$ pulse to map the transverse spin component into the z-direction, which then can be measured. In the following discussions, we describe the dynamics in the rotating frame of the Larmor frequency in which the chemical potentials of spin up and spin down are the same in the absence of interactions. In this rotating frame, the evolution of spins in the third step is dictated by the diffusion dynamics coming from interactions. Unlike the conventional use of the Ramsey sequence in the context of precision measurements, here we employ the Ramsey sequence as a probe of correlations in a 1D system.

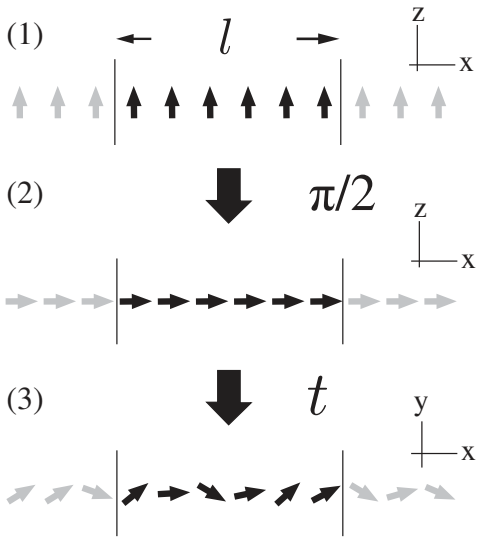

Figure 1. Ramsey sequence for the 1D system with two-component bosons considered in this paper. (1) All atoms are prepared in the spin-up state; (2) a $\pi/2$ pulse is applied to rotate each atom into the x direction; (3) spins freely evolve for time t. In actual experiments, the final $\pi/2$ pulse is applied to measure the x component of the spins. The imaging step (4) is omitted in the illustration. In this paper, spin operators refer to the ones before the final $\pi/2$ pulse.

The description of the spin dynamics starts from the highly excited state prepared after the $\pi/2$ pulse of step 2. The subsequent dynamics during step 3 crucially depends on the nature of the excitations in the system. In particular, the dynamics of a two-component Bose mixture in 1D is quite different from that in 3D. In 3D, bosons form a Bose–Einstein condensate (BEC) at low temperature, and particles occupy a macroscopic number of the $k = 0$ mode. Then, the spin diffusion of 3D BEC is dominated by the *spatially homogeneous* dynamics coming from the single $k = 0$ mode. On the other hand, bosonic systems in 1D do not have the macroscopic occupancy of the $k = 0$ mode, and their physics is dominated by strong fluctuations, to an extent that the system cannot retain long-range phase coherence even at zero temperature [41]. Thus, the spin dynamics of a 1D bosonic system necessarily involves a large number of modes with different momenta and the spin becomes *spatially inhomogeneous* during step 3 above.

Such dynamics unique to 1D can be probed by the observation of transverse spin components in the fourth step. Since we aim to capture the multi-mode nature of the dynamics in 1D, we consider the observation of spins at length scale l, given by

$$\hat{S}^a_l(t) = \int_{-l/2}^{l/2} \mathrm{d}r\, \hat{S}^a(r,t), \tag{1}$$

where $\hat{S}^a(r,t)$ with $a = x, y$ are the transverse components of spin operators after time evolution of step 3 of duration t. We assume that l is much larger than the spin healing length ξ_s and much smaller than the system size L to avoid finite size effects. Furthermore, we assume that the number of particles within the length l, N_l, is large, so that the simultaneous measurements of $\hat{S}^x_l(t)$ and $\hat{S}^y_l(t)$ are in principle possible. For large N_l, the non-commutativity of $\hat{S}^x_l$ and $\hat{S}^y_l$ gives

corrections of the order of $1/\sqrt{N_l}$ compared to the average values. In this situation, it is also possible to measure the magnitude of transverse spin components, $\hat{S}_l^{\perp} = \sqrt{(\hat{S}_l^x)^2 + (\hat{S}_l^y)^2}$, which we will extensively study in the later sections.

Due to quantum and thermal fluctuations, the measurements of $\hat{S}_l^a(t)$ give different values from shot to shot. After the $\pi/2$ pulse of step 2, the spins are prepared in the x-direction, so the average of measurements yields $\langle \hat{S}_l^x(t=0)\rangle \approx N_l/2$ and $\langle \hat{S}_l^y(t=0)\rangle \approx 0$. In the rotating frame of the Larmor frequency, the subsequent evolution does not change the expectation value of the y component so that $\langle \hat{S}_l^y(t)\rangle \approx 0$ throughout. The decay of the average $\langle \hat{S}_l^x(t)\rangle$ during the evolution in step 3 tells us the strength of spin diffusion in the system. The behavior of $\langle \hat{S}_l^a(t)\rangle$ due to spin diffusion is similar for 1D and 3D, and the difference is quantitative rather than qualitative. On the other hand, richer information about the dynamics of a 1D system is contained in the noise of $\hat{S}_l^a(t)$. Such noise inherent to quantum systems is captured by higher moments $\langle (\hat{S}_l^a(t))^n\rangle$. In this paper, we obtain the expression for the full distribution function $P_l^a(\alpha, t)$, which can produce any moments of $\hat{S}_l^a(t)$ through the relation

$$\langle (\hat{S}_l^a(t))^n\rangle = \int \mathrm{d}\alpha\ P_l^a(\alpha, t)\alpha^n, \tag{2}$$

where $P_l^a(\alpha, t)\mathrm{d}\alpha$ represents the probability that the measurement of $\hat{S}_l^a(t)$ gives the value between α and $\alpha + \mathrm{d}\alpha$. We will see in section 4 that it is also possible to obtain the joint distributions $P_l^{x,y}(\alpha, \beta, t)$ of $\hat{S}_l^x(t)$ and $\hat{S}_l^y(t)$ as well as the distribution $P_l^{\perp}(\alpha, t)$ of the squared transverse magnitude $(\hat{S}_l^{\perp})^2$.

Now we summarize the main results of this paper and give a qualitative description of spin dynamics in the Ramsey sequence. Elementary excitations of spin modes in the system are described in terms of linearly dispersing spin waves with momenta k and excitation energies $c_s|k|$, where c_s is the spin-wave velocity. When certain symmetry conditions are satisfied (see the discussion in section 4), spin and charge degrees of freedom decouple, and these spin waves are free and they do not interact among themselves in the low-energy descriptions within the so-called Tomonaga–Luttinger theory [41, 42]. Here, we describe the result in this decoupling limit, but the qualitative picture does not change even after a coupling between spin and charge is introduced, as we will see in section 5.

The initial state prepared after a $\pi/2$ pulse in step 2 in which all spins point in the x-direction is far from the equilibrium state of the system, because interactions of spins are not symmetric in terms of spin rotations. Thus, the initial state contains many excitations and the subsequent dynamics of spins is determined by the time evolution of the spin waves. A spin wave excitation with momentum k rotates spins with length scale $\sim 2\pi/k$ and time scale $\sim 1/(c_s|k|)$. The amplitude of fluctuations coming from the spin wave with momentum k is determined by the initial state as well as the nature of spin wave excitations. We find that the energy stored in each mode is approximately the same (see the discussion in section 4.2.5); thus the amplitude of fluctuations for the wave vector k scales as $1/k^2$. Therefore, the fluctuation of spins is weak at short wavelengths and short times and strong at long wavelengths and long times. In figure 2, we illustrate such dynamics of spins due to the fluctuations of spin wave excitations. It leads to the distributions presented in figures 3 and 4. Here, we have plotted the distribution function of the squared transverse magnitude of spins $(\hat{S}_l^{\perp})^2$ (figure 3) and the joint distribution function (figure 4) with $L = 200$, $K_s = 20$ and various integration lengths $l/\xi_s = 20$, 30 and 40. K_s is

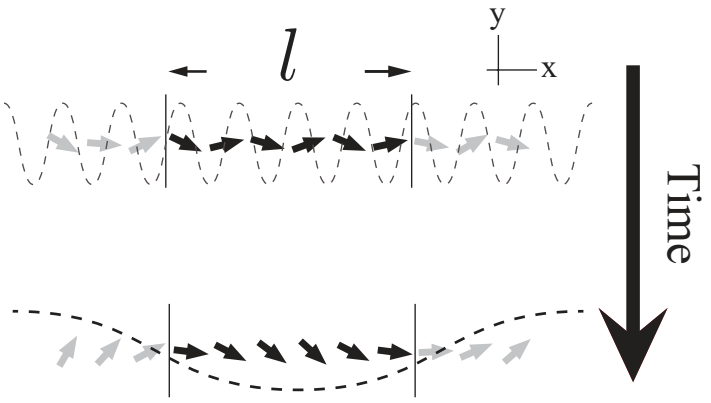

Figure 2. Illustration of the dynamics of spins in the presence of spin wave excitations. At short times (top), high momenta excitations contribute to fluctuations of the spins, but their effect is weak. At long times (bottom), low momenta excitations lead to strong fluctuations of the spins. Such fluctuations with wavelengths larger than l rotate the regions of length l as a whole so that they do not lead to decay of the magnitude of spin $\hat{S}_l^{\perp}$, but result in diffusion of $\hat{S}_l^x$.

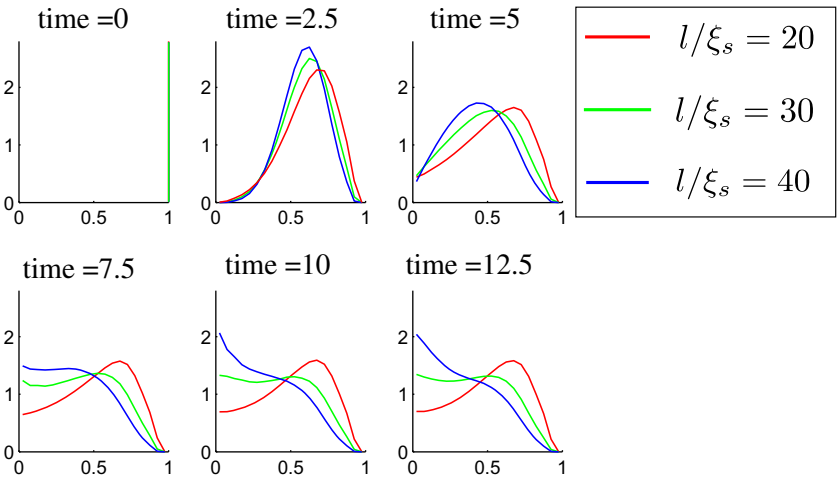

Figure 3. Time evolution of the distribution $P_l^{\perp}(\alpha)$ of the squared transverse magnitude of spins, $(\hat{S}_l^{\perp})^2$, for the system size $L/\xi_s = 200$, the spin Luttinger parameter $K_s = 20$ and various integration lengths $l/\xi_s = 20$, 30 and 40. Here ξ_s is the spin healing length, and the x-axis is scaled such that the maximum value of α is 1. Time is measured in units of ξ_s/c_s, where c_s is the spin sound wave velocity. The evolution of the distribution crucially depends on the integration length. The steady state of the distribution of the squared transverse magnitude has a peak at a finite value for a short integration length $l/\xi_s = 20$, whereas the peak is at 0 for a long integration length $l/\xi_s = 40$.

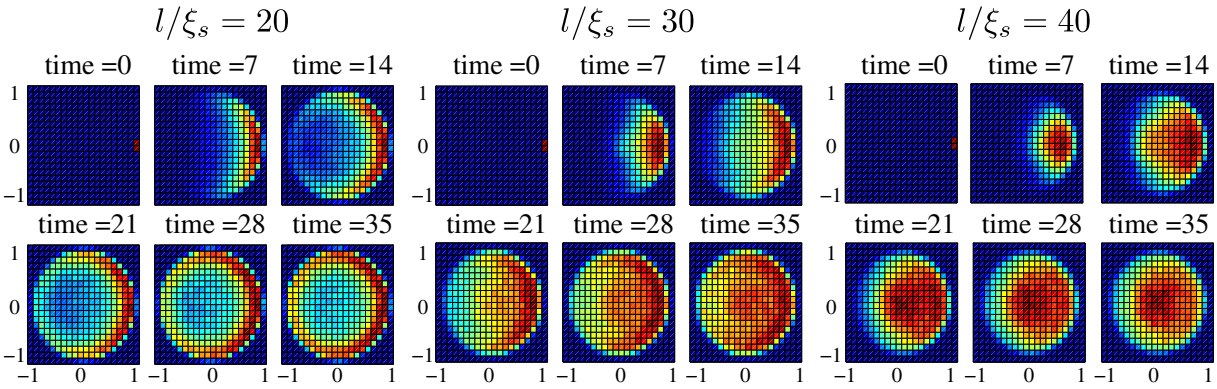

Figure 4. Time evolution of the joint distribution function $P^{x,y}(\alpha, \beta)$ for the system size $L/\xi_s = 200$, the spin Luttinger parameter $K_s = 20$ and various integration lengths $l/\xi_s = 20$ (left), 30 (middle) and 40 (right). Time is measured in units of ξ_s/c_s, where c_s is the spin sound wave velocity. Here axes are scaled such that the maximum values of α and β are 1. For for a short integration length $l/\xi_s = 20$, the dynamics leads to a distribution with the 'ring'-like structure, showing that the magnitude of spins does not decay much (spin diffusion regime). On the other hand, for longer integration lengths, the magnitude of spins decays quickly and the distribution forms a 'disc'-like structure (spin decay regime).

the spin Luttinger parameter, which measures the strength of correlations in a 1D system (see equation (8) below), and ξ_s is a spin healing length that gives a characteristic length scale in the low-energy theory of spin physics.

The multi-mode nature of a 1D system, in which spin correlations at different length scales are destroyed in a qualitatively different fashion during the dynamics, can be revealed most clearly in the squared transverse magnitude of spins $(\hat{S}_l^{\perp})^2$, plotted in figure 3. In the initial state, all the spins are aligned in the x-direction, so the distribution of $(\hat{S}_l^{\perp})^2$ is a delta function peak at its maximum value, $\sim(\rho l)^2$, where ρ is the average density of spin up or spin down. The evolution of spin waves leads to fluctuations of spins and thus to the decay of the integrated magnitude of the transverse spin. How the spin waves affect the integrated magnitude of spins strongly depends on the wavelength of the excitations. Spin excitations with momenta much smaller than $\sim 2\pi/l$ do not affect $(\hat{S}_l^{\perp})^2$ since these spin waves rotate the spins within l as a whole, while spin excitations with higher momenta lead to decay of the magnitude. This is in stark contrast with the x component of the spin $\hat{S}_l^x$, which receives contributions from spin waves of all wavelengths.

As a result of different contributions of spin-wave excitations with different wavelengths to the integrated spin magnitude, there are two distinct types of behavior of the distributions of $(\hat{S}_l^{\perp})^2$; one for short integration length l, which we call 'spin diffusion regime' and another for long integration length l, which we call 'spin decay regime'.

For short integration length l, the distribution function of $(\hat{S}_l^{\perp})^2$ is always peaked near its maximum value $(\rho l)^2$ during the dynamics because the strengths of fluctuations coming from spin waves with high momenta are suppressed by $1/k^2$ (figure 3, $l/\xi_s = 20$). While the

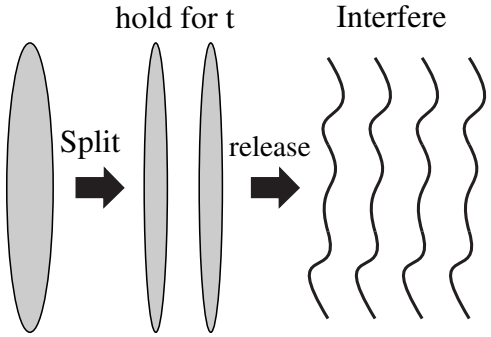

Figure 5. The interference of two quasi-condensates that are created by splitting a single quasi-condensate. After the splitting, the quasi-condensates are held for time t and then the transverse confinement is released. The two condensates interfere with each other after the release, and the position of constructive interference is denoted by a solid line in the figure. This interference pattern contains information about the local phase difference between the two quasi-condensates at the time of release.

magnitude of spins does not decay in this regime, fluctuations still lead to a diffusion of $\hat{S}_l^x$, thus, we call this regime the 'spin diffusion regime'.

On the other hand, for long integration length, spin waves lead to fluctuations of the spins within the integration region, and the spins are randomized after a long time. This randomization of spins leads to the development of a Gaussian-like peak near $(S_l^\perp)^2 = 0$ (figure 3, $l/\xi_s = 40$). During the intermediate time, both peaks at 0 and the maximum value $(\rho l)^2$ are present, and one can observe a double-peak structure. Because of the strong decaying behavior of the magnitude of spin, we call this regime the 'spin decay regime'.

More complete behavior of distribution functions can be captured by looking at the joint distribution functions from which we can read off the distributions of both $(\hat{S}_l^\perp)^2$ and $\hat{S}_l^x$; see figure 4[5]. In the 'spin diffusion regime' with short l, the joint distributions form a 'ring' during the time evolution, whereas in the 'spin decay regime' with long l, they form a 'disc'-like structure in the long-time limit. As we will see later, a dimensionless parameter given by $l_0 \sim \frac{\pi^2 l}{4K_s\xi_s}$ determines whether the dynamics belongs to the 'spin diffusion regime' ($l_0 \leqslant 1$) or the 'spin decay regime' ($l_0 \gg 1$).

We emphasize that in 3D, spin waves are dominated by the $k = 0$ mode and therefore there is almost no decay in the magnitude of spins throughout the dynamics. Therefore, the existence of two qualitatively different types of behavior of distribution functions of $(\hat{S}_l^\perp)^2$ unambiguously distinguishes the dynamics in 1D and 3D.

2.2. Dynamics of the interference between split condensates

The dynamics of the Ramsey sequence considered above can be directly mapped to the dynamics of the interference pattern of a split 1D quasi-condensate [57]. More specifically, we consider the following sequence of operations (see figure 5). Firstly, we prepare a

[5] We remark that in the previous report [52] the figure showing joint distributions contained a small error coming from an error in their numerical evaluations. Figure 4 corrects the mistake. This does not change any of the qualitative conclusions drawn in the previous work.

one-component 1D quasi-condensate in equilibrium. At time $t = 0$, the quasi-condensate is quickly split along the axial direction, and the resulting two quasi-condensates are completely separated. The two quasi-condensates freely evolve for a hold time of t, and they are released from transverse traps to observe the interference pattern between these two quasi-condensates. Such dynamics of the interference patterns as a function of hold time t has been observed in the experiment by Hofferberth *et al* [23], where the average of interference patterns is analyzed in detail. Here we study the unique 1D dynamics by looking at the full distributions of interference patterns (for an experimental study, see [24]).

The dynamics of a split condensate can be mapped to the dynamics of the Ramsey interferometer studied in this paper. The splitting of a quasi-condensate corresponds to the initial $\pi/2$ pulse in the Ramsey sequence. If we denote one of the quasi-condensates by L for left and another by R for right, the L (R) condensate corresponds to the spin-up (spin-down) component. Thus, the density difference between the two condensates corresponds to the z component of the spin, namely $\hat{S}^z(r,t) = \psi_{\mathrm{L}}^\dagger(r,t)\psi_{\mathrm{L}}(r,t) - \psi_{\mathrm{R}}^\dagger(r,t)\psi_{\mathrm{R}}(r,t)$, where $\psi_i^\dagger(r,t)$ is the creation operator of particles in the $i = \mathrm{L}$, R (R) condensate. Moreover, the local phase difference between the two condensates corresponds to the local spin direction in the x–y-plane. To see this, we first note that $\psi_{\mathrm{L}}^\dagger(r,t)\psi_{\mathrm{R}}(r,t)$ corresponds to the spin raising operator $\hat{S}^+(r,t)$. This operator is expressed in terms of the phase difference between the condensates $\hat{\phi}_{\mathrm{s}}(r,t)$ as $\hat{S}^+(r,t) \equiv \psi_{\mathrm{L}}^\dagger(r,t)\psi_{\mathrm{R}}(r,t) \sim \rho\, \mathrm{e}^{\mathrm{i}\hat{\phi}_{\mathrm{s}}(r,t)}$, where ρ is the average density of each condensate. Thus, for example, x and y spin operators are given by $\hat{S}^x(r,t) \equiv \rho\cos(\hat{\phi}_{\mathrm{s}}(r,t))$ and $\hat{S}^y(r,t) \equiv \rho\sin(\hat{\phi}_{\mathrm{s}}(r,t))$. Immediately after the splitting, the phases of the two quasi-condensates at the same coordinate along the axial direction are the same. Therefore, the splitting prepares spins in the x-direction in the language of the Ramsey sequence and thus the splitting effectively amounts to the $\pi/2$ pulse.

The interference of two quasi-condensates measures the local phase difference at time t. If the phases of L and R condensates are the same, the interference pattern has a constructive peak at the center of two condensates, which we call $x = 0$. Thus, a shift in the interference pattern measures the local phase difference between the two condensates, which yields information about $\hat{S}^x(r) = \rho\cos(\hat{\phi}_{\mathrm{s}}(r))$ as well as $\hat{S}^y(r) = \rho\sin(\hat{\phi}_{\mathrm{s}}(r))$. We note that the integrated interference contrast that can be extracted from experiments is given by the expression $\hat{C}^2 = |\rho\int_l \mathrm{e}^{\mathrm{i}\hat{\phi}_{\mathrm{s}}(r)}|^2$ [26] and is related to the transverse magnitude of spins as $(\hat{S}_l^\perp)^2 = |\hat{S}_l^x + \mathrm{i}\hat{S}_l^y|^2 = \hat{C}^2$.

All the results obtained for Ramsey dynamics are directly applicable to the dynamics of interference patterns between split condensates. When the splitting process prepares two condensates with an equal average number of particles, 'spin' and 'charge' degrees of freedom decouple, see section 6 for details. In particular, depending on the integration length of the interference patterns along the axial direction, there exist two regimes corresponding to 'phase diffusion regime' and 'contrast decay regime', analogous to the 'spin diffusion regime' and 'spin decay regime' described in the previous section, respectively.

2.3. Prethermalization of 1D condensates

The equilibration and relaxation dynamics of generic many-body systems are fundamental open problems. Among possible processes, it has been suggested that the time evolution of some systems prepared in non-equilibrium states results in the attainment of quasi-steady states within a much shorter time than equilibration time. This quasi-steady state is often not a true

equilibrium state, but rather it is a dephased state, and true equilibration takes place at a much longer time scale. Yet in some cases, the physical observables in the quasi-steady states take a value corresponding to the one in thermal equilibrium at some effective temperature $T_{\rm eff}$, displaying disguised 'thermalized' states. Such surprising non-equilibrium phenomena, called prethermalization, have been predicted to occur in quantum as well as classical many-body systems [58–60] and were observed in [24].

In particular, integrable 1D systems are known *not to* thermalize, and indeed, experiments in [47] have observed an exceedingly long equilibration time. Yet even in this extreme case, we suggest in this section that many-body 1D systems can reach disguised 'thermalized' states through prethermalization phenomena within a short time.

The Ramsey dynamics and dynamics of interference patterns between split condensates described in the previous sections are particular examples of dynamics in which slow equilibration is expected because the system essentially consists of uncoupled harmonic oscillators in the low-energy description (see section 4). In the following, we give a heuristic argument that the distribution of the interference contrast amplitudes of the two *non-equilibrium* quasi-condensates is given by that of two *equilibrium* quasi-condensates at some effective temperature $T_{\rm eff}$. More details can be found in section 6.3.

A long time after the splitting, the position of the interference peak becomes completely random, and yields no information. Therefore, we focus on the squared transverse magnitude of the spin $(\hat{S}_l^{\perp})^2$, or equivalently, the interference contrasts $\hat{C}^2$. In the following, we describe the physics for the dynamics of split condensates, but the same argument can be applied to Ramsey dynamics. The interference contrast of the split condensates after a long time is determined by the 'average' phase fluctuations present in the system. In the dephased limit, such fluctuations are determined by the total energy present in each mode labeled by momenta k. Now for sufficiently fast splitting, the energy $E_{\rm split}$ contained in each mode is independent of momenta because the density difference of quasi-condensates along the axial direction is uncorrelated in the initial state beyond the spin healing length $\xi_{\rm s}$ (see the discussion below equation (10)). On the other hand, the interference contrast of *thermal* condensates at temperature T is determined by the thermal phase fluctuations caused by excitations whose energy is distributed according to equipartition theorem; each mode in the *thermal* condensates contains equal energy of $k_{\rm B}T$. Thus, from this argument, we find that the interference contrast of split condensates after a long time becomes indistinguishable from the one resulting from thermal condensates at temperature $k_{\rm B}T_{\rm eff} = E_{\rm split}$. We will show in section 6.3 that in fact the *full distribution function* of interference contrast becomes indistinguishable for these two states. In the case of splitting 2D condensates, equipartition of energy and the existence of 'non-equilibrium temperature' were pointed out in [60].

Here we propose the occurrence of such prethermalization within the Tomonaga–Luttinger theory. We emphasize that within the Tomonaga–Luttinger theory of low-energy excitations, different modes are decoupled and therefore no true thermalization can take place. In realistic experimental situations, such integrability can be broken and relaxation and thermalization processes are expected to occur after long time dynamics. The requirement to observe the prethermalization phenomena predicted in this theory in experiments depends on the time scale of other possible thermalization processes we did not consider in our model, such as effective three-body collisions [61, 62], relaxation of high-energy quasi-particles [63], or interactions among the collective modes through anharmonic terms we neglected in the Tomonaga–Luttinger theory [64]. When all these processes occur at much slower time scales

than the prethermalization time scale, which is roughly given by the integration length divided by the spin sound velocity $\sim l/c_s$ for the decoupling case, the observation of prethermalization should be possible. In 1D, the dynamics is strongly constrained due to the conservation of energy and momentum, and therefore it is likely that the dynamics is dominated by the modes described by the Tomonaga–Luttinger theory for a long time for quasi-condensates with low initial temperatures.

Such prethermalizations are expected to occur even in higher-dimensional systems [19, 25, 60, 65]. We note that the conditions for the experimental observations of the phenomena might be more stringent because true thermalization processes are expected to take place much more quickly in 2D and 3D systems.

3. Two-component Bose mixtures in 1D: the Hamiltonian

In this paper, we study the dynamics of two-component Bose mixtures in 1D through the Tomonaga–Luttinger formalism [41, 42]. As we have stated before, we assume the rotating frame in which spin-up and spin-down particles have the same chemical potential in the absence of interactions. The Hamiltonian of two-component Bose mixtures in 1D is given by

$$\mathcal{H} = \int_{-L/2}^{L/2} \mathrm{d}r \left[\sum_i \frac{1}{2m_i} \nabla\psi_i^\dagger(r)\nabla\psi_i(r) + \sum_{ij} g_{ij}\, \psi_i^\dagger(r)\psi_j^\dagger(r)\psi_j(r)\psi_i(r) \right]. \tag{3}$$

Here ψ_i with $i = \uparrow, \downarrow$ describe two atomic species with masses m_i, and g_{ij} are the interaction strengths given by $g_{ij} = \nu_\perp a_{ij}$ [66] where $\nu_\perp$ is the frequency of transverse confinement potential and a_{ij} are the scattering lengths between spins i and j. The system size is taken to be L, and we take the periodic boundary condition throughout the paper. In addition, we use the units in which $\hbar = 1$.

In the low-energy description, the Hamiltonians for weakly interacting bosons after the initial $\pi/2$ rotation can be written in quadratic form, and are given by

$$\begin{aligned} H &= H_\uparrow + H_\downarrow + H_{\mathrm{int}}, \\ H_\uparrow &= \int_{-L/2}^{L/2} \mathrm{d}r \left[\frac{\rho}{2m_\uparrow} (\nabla\hat{\phi}_\uparrow(r))^2 + g_{\uparrow\uparrow}(\hat{n}_\uparrow(r))^2 \right], \\ H_\downarrow &= \int_{-L/2}^{L/2} \mathrm{d}r \left[\frac{\rho}{2m_\downarrow} (\nabla\hat{\phi}_\downarrow(r))^2 + g_{\downarrow\downarrow}(\hat{n}_\downarrow(r))^2 \right], \\ H_{\mathrm{int}} &= 2\int_{-L/2}^{L/2} \mathrm{d}r(r)[g_{\uparrow\downarrow}\hat{n}_\uparrow\hat{n}_\downarrow(r) + g^\phi_{\uparrow\downarrow}\nabla\hat{\phi}_\uparrow\nabla\hat{\phi}_\downarrow(r)], \end{aligned} \tag{4}$$

where ρ is the average density of each species and $\hat{n}_\sigma$ are variables representing the phase and density fluctuations for the particle with spin σ. These variables obey a canonical commutation relation $[\hat{n}_\sigma(r), \hat{\phi}_\sigma(r')] = -\mathrm{i}\delta(r - r')$. In the Hamiltonian above, we included the kinetic interaction term $g^\phi_{\uparrow\downarrow}$, which is zero for weakly interacting bosons, but allowed by inversion symmetry and non-zero for generic Tomonaga–Luttinger Hamiltonians.

We note that in the weakly interacting case, one can obtain the parameters of the Hamiltonian in equation (4) such as g_{ij} and m_i through hydrodynamic linearization of the microscopic Hamiltonian. In this case, we assume the small fluctuations of the densities $\hat{n}_\sigma$ and phases $\nabla\hat{\phi}_\sigma$ and expand the Hamiltonian in equation (3) to the second order in these variables through the expression $\psi_\sigma^\dagger \sim \sqrt{\rho+\hat{n}_\sigma}\, e^{i\hat{\phi}_\sigma}$, resulting in the form of the Hamiltonian in equation (4). Due to these assumptions of small spatial variations of the phase, $\hat{n}_\sigma$ and $\hat{\phi}_\sigma$ represent the 'coarse-grained' variables where collective modes have linear dispersions. The Hamiltonian of the Tomonaga–Luttinger theory in equation (4) can also describe the effective low-energy physics of strongly interacting systems, but in this case there is no simple relation between microscopic parameters and the parameters of the Hamiltonian in equation (4).

In order to describe the spin dynamics, we define spin and charge operators as the difference and the sum of spin-up and -down operators, i.e. $\hat{\phi}_\mathrm{s} = \hat{\phi}_\uparrow - \hat{\phi}_\downarrow$, $\hat{\phi}_\mathrm{c} = \hat{\phi}_\uparrow + \hat{\phi}_\downarrow$, $\hat{n}_\mathrm{s} = \frac{1}{2}(\hat{n}_\uparrow - \hat{n}_\downarrow)$, $\hat{n}_\mathrm{c} = \frac{1}{2}(\hat{n}_\uparrow + \hat{n}_\downarrow)$. In this representation, the Hamiltonian in equation (4) becomes

$$
\begin{aligned}
H &= H_\mathrm{s} + H_\mathrm{c} + H_\mathrm{mix},\\
H_\mathrm{s} &= \int_{-L/2}^{L/2} \mathrm{d}r \left[\frac{\rho}{2m_\mathrm{s}}(\nabla\hat{\phi}_\mathrm{s}(r))^2 + g_\mathrm{s}(\hat{n}_\mathrm{s}(r))^2\right], \qquad (5)\\
H_\mathrm{c} &= \int_{-L/2}^{L/2} \mathrm{d}r \left[\frac{\rho}{2m_\mathrm{c}}(\nabla\hat{\phi}_\mathrm{c}(r))^2 + g_\mathrm{c}(\hat{n}_\mathrm{c}(r))^2\right], \qquad (6)\\
H_\mathrm{mix} &= 2\int_{-L/2}^{L/2} \mathrm{d}r [g_\mathrm{mix}\hat{n}_\mathrm{s}(r)\hat{n}_\mathrm{c}(r) + g_\mathrm{mix}^\phi \nabla\hat{\phi}_\mathrm{s}(r)\nabla\hat{\phi}_\mathrm{c}(r)], \qquad (7)
\end{aligned}
$$

where interaction strengths are given by $g_\mathrm{c} = g_{\uparrow\uparrow} + g_{\downarrow\downarrow} + 2g_{\uparrow\downarrow}$, $g_\mathrm{s} = g_{\uparrow\uparrow} + g_{\downarrow\downarrow} - 2g_{\uparrow\downarrow}$, $g_\mathrm{mix} = g_{\uparrow\uparrow} - g_{\downarrow\downarrow}$, $g_\mathrm{mix}^\phi = \rho/(8m_\uparrow) - \rho/(8m_\downarrow)$. The masses are given by the relations $\rho/(2m_\mathrm{c}) = \rho/(8m_\uparrow) + \rho/(8m_\downarrow) + g_{\uparrow\downarrow}^\phi/2$ and $\rho/(2m_\mathrm{s}) = \rho/(8m_\uparrow) + \rho/(8m_\downarrow) - g_{\uparrow\downarrow}^\phi/2$.

The spin variables $\hat{\phi}_\mathrm{s}$ and $\hat{n}_\mathrm{s}$ are 'coarse-grained' in the sense that they represent the operators in the long wavelength beyond the spin healing length ξ_s. ξ_s is determined from microscopic physics and gives the length below which the kinetic energy of spins wins over the interaction energy, see equation (5) above. For weakly interacting bosons with $m_\uparrow = m_\downarrow = m$, it is given by $\xi_\mathrm{s} = \pi/\sqrt{m\rho g_\mathrm{s}}$. In the following, we assume that the number of particles within the spin healing length is large, i.e. $\xi_\mathrm{s}\rho \gg 1$. This condition is always satisfied for weakly interacting bosons.

In the next section, we consider the case $g_\mathrm{mix} = 0$ and $g_\mathrm{mix}^\phi = 0$, in which spin and charge degrees of freedom decouple. Then the dynamics of spins is completely described by the spin Hamiltonian in equation (5). The general case where $g_\mathrm{mix} \neq 0$ and $g_\mathrm{mix}^\phi \neq 0$ will be treated in section 5.

4. Dynamics of full distribution functions for decoupled spin and charge degrees of freedom

4.1. The Hamiltonian and the initial state

The experiment of Widera *et al* [22] used $F = 1$, $m_F = +1$ and $F = 2$, $m_F = -1$ states of ^{87}Rb for spin-up and spin-down particles, respectively. These hyperfine states have the scattering

lengths $a_{\sigma\sigma'}$ such that $a_{\uparrow\uparrow} \approx a_{\downarrow\downarrow}$. Consequently, the mixing Hamiltonian in equation (7) approximately vanishes for weak interactions. Motivated by this experiment, here we consider the decoupling of spin and charge degrees of freedom [52]. Spin dynamics in this case is completely determined by the spin Hamiltonian

$$H_{\rm s} = \frac{c_{\rm s}}{2} \int \left[\frac{K_{\rm s}}{\pi} (\nabla \hat{\phi}_{\rm s}(r))^2 + \frac{\pi}{K_{\rm s}} \hat{n}_{\rm s}^2(r) \right] {\rm d}r, \tag{8}$$

where $K_{\rm s}$ is the spin Luttinger parameter representing the strength of interactions, and $c_{\rm s}$ is the spin sound velocity. $K_{\rm s}$ and $c_{\rm s}$ are directly related to the spin healing length $\xi_{\rm s}$ in the weak-interaction limit, given by $2K_{\rm s} = \rho\xi_{\rm s}$ and $c_{\rm s} = \frac{\pi}{2m_{\rm s}\xi_{\rm s}}$. Note that $\hat{n}_{\rm s}(r,t)$ is the local spin imbalance $\hat{n}_{\rm s} = \psi_\alpha^\dagger(\frac{1}{2}\sigma^z_{\alpha\beta})\psi_\beta$ and $\hat{\phi}_{\rm s}(r,t)$ is related to the direction of the transverse spin component $\rho\, {\rm e}^{{\rm i}\hat{\phi}_{\rm s}} = \psi_\alpha^\dagger \sigma^+_{\alpha\beta}\psi_\beta$. Here, $\psi_\alpha^\dagger$ is the creation operator of spin $\alpha = \uparrow, \downarrow$. These variables $\hat{n}_{\rm s}$ and $\hat{\phi}_{\rm s}$ obey a canonical commutation relation $[\hat{n}_{\rm s}(r), \hat{\phi}_{\rm s}(r')] = -{\rm i}\delta(r-r')$.

Other spin variables can be similarly defined in terms of coarse-grained spin variables $\hat{n}_{\rm s}$ and $\hat{\phi}_{\rm s}$. In the following, we consider the general transverse spins pointing in the direction $(x, y, z) = (\cos\theta, \sin\theta, 0)$ integrated over l given by

$$\begin{aligned} \hat{S}_l^\theta &= \int_{-l/2}^{l/2} {\rm d}r\, \psi_\alpha^\dagger(r,t) \left(\cos\theta \frac{\sigma^x_{\alpha\beta}}{2} + \sin\theta \frac{\sigma^y_{\alpha\beta}}{2} \right) \psi_\beta(r,t) \\ &= \int_{-l/2}^{l/2} {\rm d}r \frac{\rho}{2} ({\rm e}^{{\rm i}(\hat{\phi}_{\rm s}(r)-\theta)} + {\rm e}^{-{\rm i}(\hat{\phi}_{\rm s}(r)-\theta)}), \end{aligned} \tag{9}$$

where σ^a with $a = x, y$ are Pauli matrices. Here, $\hat{S}_l^\theta$ with $\theta = 0$ corresponds to spin x operator and $\theta = \pi/2$ corresponds to spin y operator. In order to explore the 1D dynamics resulting from the Hamiltonian in equation (8), we analytically compute the mth moment of the spin operator $\hat{S}_l^\theta$, $\langle (\hat{S}_l^\theta)^m \rangle$, after time t of the $\pi/2$ pulse of the Ramsey sequence. Then, the full distribution functions of $\hat{S}_l^x$ and $\hat{S}_l^y$, as well as the joint distribution of these, will be obtained from $\langle (\hat{S}_l^\theta)^m \rangle$.

In order to study the dynamics of Ramsey interferometer in terms of low-energy variables $\hat{n}_{\rm s}$ and $\hat{\phi}_{\rm s}$, we need to write down an appropriate state after the $\pi/2$ pulse in terms of $\hat{n}_{\rm s}$ and $\hat{\phi}_{\rm s}$. If the pulse is sufficiently strong, each spin is independently rotated into the x-direction after the $\pi/2$ pulse. Naively, this prepares the initial state in the eigenstate of $\hat{S}^x(r) = \rho\cos\hat{\phi}_{\rm s}(r)$ with eigenvalue $\hat{\phi}_{\rm s}(r) = 0$. However, due to the commutation relation between $\hat{n}_{\rm s}$ and $\hat{\phi}_{\rm s}$, such an initial state has an infinite fluctuation in $\hat{n}_{\rm s}$ and therefore the state has infinite energy according to equation (8). This unphysical consequence comes about because the low-energy theory in equation (8) should not be applied to the physics of a short time scale given by $1/E_{\rm c}$, where $E_{\rm c}$ is the high-energy cutoff of the Tomonaga–Luttinger theory. During this short time dynamics, the initial state establishes the correlation at the length scale of spin healing length $\xi_{\rm s}$. The state after this short time dynamics can now be described in terms of the coarse-grained variables $\hat{n}_{\rm s}(r)$ and $\hat{\phi}_{\rm s}(r)$. The variables $\hat{n}_{\rm s}(r)$ and $\hat{\phi}_{\rm s}(r)$ are defined on a length scale larger than the spin healing length $\xi_{\rm s}$. Since the z component of spins is still uncorrelated beyond $\xi_{\rm s}$ after the initial short time dynamics, the appropriate initial condition of the state is written as

$$\langle S^z(r) S^z(r') \rangle = \langle \hat{n}_{\rm s}(r) \hat{n}_{\rm s}(r') \rangle = \frac{\rho\eta}{2} \delta(r-r'), \tag{10}$$

where the delta function $\delta(r-r')$ should be understood as a smeared delta function over the scale of $\xi_{\rm s}$. Because the state after the short time dynamics is still close to the eigenstate

of the $\hat{S}^x(r)$ operator, spins are equal superpositions of spin up and spin down. Then the distribution of $\hat{S}^z_l = \int_0^l \hat{S}^z(r)\,\mathrm{d}r$ is determined through random picking of the values $\pm 1/2$ for $2\rho l$ particles. Due to the central limit theorem, the distribution of $\hat{S}^z_l = \int_0^l \hat{S}^z(r)\,\mathrm{d}r$ is Gaussian, i.e. $\langle (\hat{S}^z_l)^{2n}\rangle = \frac{(2n)!}{2^n n!}(\rho l \eta/2)^n$. In particular, $\langle (\hat{S}^z_l)^2\rangle = \rho l \eta/2$, which determines the magnitude of the fluctuation for $\hat{S}^z(r)$ in equation (10). In equation (10), we also introduced the phenomenological parameter η, which accounts for the decrease and increase of fluctuations coming from, for example, imperfections of the $\pi/2$ pulse. The ideal, fast application of a $\pi/2$ pulse corresponds to $\eta = 1$. In the experimental realization of [22], η was determined to be between 0.8 and 1.3 through the fitting of the experiment with the Tomonaga–Luttinger theory for the time evolution of the average x component of the spin, $\langle \hat{S}^x_l\rangle$. Through the engineering of the initial state such as the application of a weak $\pi/2$ pulse, η can also be made intentionally smaller than 1.

A convenient basis to describe the initial state of the dynamics above is the basis that diagonalizes the spin Hamiltonian of equation (8). The phase and density of the spins $\hat{\phi}_\mathrm{s}(r)$ and $\hat{n}_\mathrm{s}(r)$ can be written in terms of the creation $b^\dagger_{\mathrm{s},k}$ and annihilation $b_{\mathrm{s},k}$ operators of elementary excitations for the spin Hamiltonian in equation (8) as

$$\begin{aligned}
\hat{\phi}_\mathrm{s}(r) &= \frac{1}{\sqrt{L}}\sum_k \hat{\phi}_{\mathrm{s},k}\,\mathrm{e}^{\mathrm{i}kr} = \frac{1}{\sqrt{L}}\left(\sum_{k\neq 0} -\mathrm{i}\sqrt{\frac{\pi}{2|k|K_\mathrm{s}}}(b^\dagger_{\mathrm{s},k} - b_{\mathrm{s},-k})\mathrm{e}^{\mathrm{i}kr} + \hat{\phi}_{\mathrm{s},0}\right),\\
\hat{n}_\mathrm{s}(r) &= \frac{1}{\sqrt{L}}\sum_k \hat{n}_{\mathrm{s},k}\,\mathrm{e}^{\mathrm{i}kr} = \frac{1}{\sqrt{L}}\left(\sum_{k\neq 0} \sqrt{\frac{|k|K_\mathrm{s}}{2\pi}}(b^\dagger_{\mathrm{s},k} + b_{\mathrm{s},-k})\mathrm{e}^{\mathrm{i}kr} + \hat{n}_{\mathrm{s},0}\right),\\
\mathcal{H}_\mathrm{s} &= \sum_{k\neq 0} c_\mathrm{s}|k| b^\dagger_{\mathrm{s},k} b_{\mathrm{s},k} + \frac{\pi c_\mathrm{s}}{2K_\mathrm{s}}\hat{n}^2_{\mathrm{s},0},
\end{aligned} \tag{11}$$

where we have defined $\hat{\phi}_{\mathrm{s},k}$ and $\hat{n}_{\mathrm{s},k}$ as the Fourier transforms of operators $\hat{\phi}_\mathrm{s}(r)$ and $\hat{n}_\mathrm{s}(r)$. Note that $b^\dagger_{\mathrm{s},k}$ creates a collective mode with momentum k and follows a canonical commutation relation $[b_{\mathrm{s},k}, b^\dagger_{\mathrm{s},k}] = 1$. Note that the $k = 0$ mode has no kinetic energy, and it naturally has a different evolution than $k \neq 0$ modes.

The Gaussian state determined by equation (10) takes the form of a squeezed state of operators $b_{\mathrm{s},k}$, and it is given by

$$\begin{aligned}
|\psi_0\rangle &= \frac{1}{\mathcal{N}}\exp\left(\sum_{k\neq 0} W_k b^\dagger_{\mathrm{s},k} b^\dagger_{\mathrm{s},-k}\right)|0\rangle|\psi_{\mathrm{s},k=0}\rangle,\\
\langle n_{\mathrm{s},0}|\psi_{\mathrm{s},k=0}\rangle &= \exp\left(-\frac{1}{2\rho\eta}n^2_{\mathrm{s},0}\right),
\end{aligned} \tag{12}$$

where $2W_k = \frac{1-\alpha_k}{1+\alpha_k}$ and $\alpha_k = \frac{|k|K_\mathrm{s}}{\pi\rho\eta}$. Here the state $|n_{\mathrm{s},0}\rangle$ is the normalized eigenstate of the operator $\hat{n}_{\mathrm{s},0}$ with eigenvalue $n_{\mathrm{s},0}$. The summation of k in the exponent has an ultraviolet

cutoff around $k_c = 2\pi/\xi_s$. $\mathcal{N}$ is the overall normalization of the state. It is easy to check that $\langle\psi_0|\hat{n}_{s,k}\hat{n}_{s,k'}|\psi_0\rangle = \frac{\rho\eta}{2}\delta_{k,-k'}$, which corresponds to equation (10).

4.2. Moments and full distribution functions of spins

After the free evolution of the initial state $|\psi_0\rangle$ for time t, the state becomes $|\psi(t)\rangle = e^{-iH_s t}|\psi_0\rangle$. We characterize the state at time t by the mth moments of spin operators, $\langle(\hat{S}_l^\theta)^m\rangle$. As we will see below, the full distribution function can be constructed from the expression of $\langle(\hat{S}_l^\theta)^m\rangle$ [18].

We consider the evaluation of moments $\langle(\hat{S}_l^\theta)^m\rangle$ at time t, $|\psi(t)\rangle$. Each momentum k component of the initial state $|\psi_0\rangle$ independently evolves in time. Since the $k = 0$ mode has a distinct evolution from other $k \neq 0$ modes, we separately consider $k = 0$ and $k \neq 0$ modes.

4.2.1. The $k = 0$ mode. The Hamiltonian of the $k = 0$ mode is given by $H_{s,k=0} = \frac{\pi c_s}{2K_s}\hat{n}_{s,0}^2$ in equation (11). Therefore, in the basis of $n_{s,0}$, the $k = 0$ part of the state $|\psi(t)\rangle$ is given by

$$\langle n_{s,0}|e^{-iH_{s,k=0}t}|\psi_{k=0}\rangle = \frac{1}{\mathcal{N}_{k=0}}\exp\left\{\left(-\frac{1}{(2\rho\eta)} - i\frac{\pi c_s t}{2K_s}\right)n_{s,0}^2\right\}, \tag{13}$$

where $\mathcal{N}_{k=0}$ is the normalization of the state. The initial Gaussian state of $\hat{n}_{s,0}$ stays Gaussian at all times, and any analytic operator of $\phi_{s,0}$ and $n_{s,0}$ can be exactly evaluated through Wick's theorem. For example, the $k = 0$ part contributes to the decay of the average of the x component of spin $\langle\hat{S}_l^x\rangle_{k=0} = l\rho\mathrm{Re}(\langle e^{i\phi_{s,0}/\sqrt{L}}\rangle)$ as

$$\begin{aligned}\langle\hat{S}_l^x\rangle_{k=0} &= l\rho\, e^{-\frac{1}{2L}\langle\phi_{s,0}^2\rangle_t},\\ \langle\phi_{s,0}^2\rangle_t &= \frac{1}{2\rho\eta} + \left(\frac{c_s\pi t}{K_s}\right)^2\frac{\eta\rho}{2}.\end{aligned} \tag{14}$$

This diffusion of the spin from the $k = 0$ contribution is generally present in any dimensional systems and is not particular to one dimension. The physical origin of this diffusion is the interaction dependent on the total spin, $\hat{S}_z^2$. The eigenstate of $\hat{S}_x$ with eigenvalue ρl is the superposition of different eigenstates of $\hat{S}_z$ with eigenvalues m_z, and they accumulate different phases $e^{-itm_z^2}$ in time. This leads to decay of $\langle\hat{S}_x\rangle$. In the thermodynamic limit $L \to \infty$, the uncertainty of $\hat{S}_z$ becomes diminishingly small, and therefore, the decay of $\langle\hat{S}_x\rangle$ coming from $k = 0$ goes to zero. More interesting physics peculiar to 1D systems comes from $k \neq 0$ modes. In the case of 3D systems, macroscopic occupancy of a single-particle state is absent in 1D, so $k \neq 0$ momentum excitations have a much more significant effect in 1D dynamics.

4.2.2. $k \neq 0$ contribution. The exact evaluation of spin moments $\langle(\hat{S}_l^\theta)^m\rangle$ for $k \neq 0$ is possible through the following trick. Consider the annihilation operator $\gamma_{s,k}(t)$ for the state $|\psi(t)\rangle$ such that $\gamma_{s,k}(t)|\psi(t)\rangle = 0$. If we write the operators $\hat{\phi}_s(r)$ in terms of $\gamma_{s,k}(t)$ and $\gamma_{s,k}^\dagger(t)$, then the $k \neq 0$ part of the mth moment schematically takes the form $\langle(\hat{S}_l^\theta)^m\rangle \sim \langle\exp(i\sum_{k\neq 0} C_{s,k}\gamma_{s,k} + C_{s,k}^*\gamma_{s,k}^\dagger)\rangle$ (here and in the following, we drop the time dependence of $\gamma_{s,k}(t)$ from the notation). Using the property $e^{\gamma_{s,k}}|\psi(t)\rangle = (1 + \gamma_{s,k} + \ldots)|\psi(t)\rangle = |\psi(t)\rangle$ and the identity $e^{A+B} = e^A e^B e^{-\frac{1}{2}[A,B]}$ where $[A, B]$ is a c-number, we can evaluate the mth moments as $\langle(S_l^\theta)^m\rangle \sim \langle e^{iC_{s,k}^*\gamma_{s,k}^\dagger} e^{-\frac{1}{2}\sum_{k\neq 0}|C_{s,k}|^2} e^{iC_{s,k}\gamma_{s,k}}\rangle = \exp(-\frac{1}{2}\sum_{k\neq 0}|C_{s,k}|^2)$.

It is straightforward to check that $\gamma_{s,k}$ operator is given by a linear combination of $b_{s,k}$ and $b^{\dagger}_{s,-k}$ as follows:

$$\begin{pmatrix} \gamma^{\dagger}_{s,-k}(t) \\ \gamma_{s,k}(t) \end{pmatrix} = \begin{pmatrix} \dfrac{e^{-ic_s|k|t}}{\sqrt{1-4|W_k|^2}} & \dfrac{-2W_k e^{ic_s|k|t}}{\sqrt{1-4|W_k|^2}} \\ \dfrac{-2W_k e^{-ic_s|k|t}}{\sqrt{1-4|W_k|^2}} & \dfrac{e^{ic_s|k|t}}{\sqrt{1-4|W_k|^2}} \end{pmatrix} \begin{pmatrix} b^{\dagger}_{s,-k} \\ b_{s,k} \end{pmatrix}. \tag{15}$$

$\gamma_{s,k}$ and $\gamma^{\dagger}_{s,k}$ obey a canonical commutation relation $[\gamma_{s,k}, \gamma^{\dagger}_{s,k}] = 1$. In terms of these $\gamma_{s,k}$, the expression of $\hat{\phi}_{s,k}(t)$ becomes

$$\begin{aligned} &\frac{1}{\sqrt{L}}\hat{\phi}_{s,k} = C_{s,k}\gamma^{\dagger}_{s,k} + C^{*}_{s,k}\gamma_{s,-k}, \\ &C_{s,k} = -i\sqrt{\frac{\pi}{2|k|K_s L}}\frac{e^{ic_s|k|t} - 2W_k\, e^{-ic_s|k|t}}{\sqrt{1-4|W_k|^2}}. \end{aligned} \tag{16}$$

$C_{s,k}(t)$ measures the fluctuation, or variance, of phase in the kth mode at time t, given by $\langle|\hat{\phi}_{s,k}(t)|^2\rangle = \langle\hat{\phi}_{s,k}(t)\hat{\phi}_{s,-k}(t)\rangle$. Indeed, since $\gamma_{s,k}$ is the annihilation operator of our state at time t, we immediately conclude that $\langle|\hat{\phi}_{s,k}(t)|^2\rangle/L = |C_{s,k}(t)|^2$.

Using the technique described above, the mth moment of $\hat{S}^{\theta}_{l}$ becomes (we include both $k = 0$ and $k \neq 0$ contributions in the expression below)

$$\begin{aligned} \langle\psi(t)|\left(\int_{-l/2}^{l/2} S^{\theta}(r)\mathrm{d}r\right)^m|\psi(t)\rangle &= \left\langle\prod_i^m\left(\int_{-l/2}^{l/2}\frac{\rho}{2}\mathrm{d}r_i\sum_{s_i=\pm1} e^{is_i(\hat{\phi}_s(r_i)-\theta)}\right)\right\rangle \\ &= \sum_{\{s_i=\pm1\}}\prod_{i=1}^m\int_{-l/2}^{l/2}\frac{\rho\,\mathrm{d}r_i}{2}\langle e^{(i(s_1\hat{\phi}_s(r_1)+\cdots+s_m\hat{\phi}_s(r_m))}\rangle e^{-i(\sum_i s_i)\theta} \\ &= \sum_{\{s_i=\pm1\}}\prod_{i=1}^m\int_{-l/2}^{l/2}\frac{\rho\,\mathrm{d}r_i}{2}\exp\left(-\frac{1}{2}\sum_k \xi^{\{s_i,r_i\}}_{s,k}(\xi^{\{s_i,r_i\}}_{s,k})^*\right)e^{-i(\sum_i s_i)\theta}, \end{aligned} \tag{17}$$

where $\xi^{\{s_i,r_i\}}_{s,k} = \sqrt{\frac{\langle|\hat{\phi}_{s,k}(t)|^2\rangle}{L}}(s_1\, e^{ikr_1} + \cdots + s_m\, e^{ikr_m})$. s_i takes either the value 1 or -1, and $\sum_{\{s_i\}}$ sums over all possible sets of values. Note that L is the total system size and l the integration range.

4.2.3. Full distribution functions. The calculation of the full distribution functions from moments in equation (17) is studied by the techniques introduced in [18] through mapping to the statistics of random surfaces. In this subsection, we provide details of the calculation.

Equation (17) is simplified if the integrations for each r_i can be independently carried out. This is not possible in equation (17) because e^{ikr_i} and e^{ikr_j} for $i \neq j$ are coupled in

$|\xi_{s,k}^{\{s_i,r_i\}}|^2 = (\mathrm{Re}\,\xi_{s,k}^{\{s_i,r_i\}})^2 + (\mathrm{Im}\,\xi_{s,k}^{\{s_i,r_i\}})^2$. To disentangle this, we introduce the Hubbard–Stratonovich transformation, $e^{-\frac{x^2}{2}} = \frac{1}{\sqrt{2\pi}}\int_{-\infty}^{\infty} e^{-\frac{\lambda^2}{2}} e^{ix\lambda}$, for example,

$$e^{-\frac{1}{2}(\mathrm{Re}(\xi_{s,k}^{\{s_i,x_i\}}))^2} = \int_{-\infty}^{\infty} \frac{d\lambda_{1sk}}{\sqrt{2\pi}} e^{-\lambda_{1sk}^2/2}\, e^{i\lambda_{1sk}\mathrm{Re}(\xi_{s,k}^{\{s_i,x_i\}})}.$$

We apply a similar transformation for $\mathrm{Im}\xi_{s,k}$. This removes the cross term between e^{ikr_i} and e^{ikr_j} for $i \neq j$ and allows us to independently integrate over r_i's. Associated with each transformation, we introduce auxiliary variables λ_{1sk} for $\mathrm{Re}(\xi_{s,k})$ and λ_{2sk} for $\mathrm{Im}(\xi_{s,k})$. Then, the mth moment becomes

$$\langle\psi(t)|\left(\int_{-l/2}^{l/2} S^{\theta}(r)dr\right)^m |\psi(t)\rangle = \sum_{\{s_i\}}\prod_k \int_{-\infty}^{\infty} e^{-(\lambda_{1sk}^2+\lambda_{2sk}^2)/2}\frac{d\lambda_{1sk}}{\sqrt{2\pi}}\frac{d\lambda_{2sk}}{\sqrt{2\pi}} \times\left[\prod_{i=1}^{m}\int_{-l/2}^{l/2}\frac{\rho\, dr_i}{2}\exp\left(is_i\sum_k\left\{\lambda_{1sk}\mathrm{Re}(\xi_{s,k}^{r_i}) + \lambda_{2sk}\mathrm{Im}(\xi_{s,k}^{r_i}) - \theta\right\}\right)\right],$$

where we introduced $\xi_{s,k}^{\{r_i\}} = \sqrt{\frac{\langle|\hat{\phi}_{s,k}(t)|^2\rangle}{L}}\, e^{ikr_i}$. Summation over $\{s_i = \pm 1\}$ can now be carried out. Furthermore, we introduce new variables λ_{rsk} and $\lambda_{\theta sk}$, and replace λ_{1sk} and λ_{2sk} through the relations $\lambda_{rsk} = \sqrt{\lambda_{1sk}^2 + \lambda_{2sk}^2}$ and $\cos(\lambda_{\theta sk}) = \lambda_{2sk}/\sqrt{\lambda_{1sk}^2 + \lambda_{2sk}^2}$. These operations result in the simplified expression

$$\langle\psi(t)|\left(\int_{-l/2}^{l/2} S^{\theta}(r)dr\right)^m |\psi(t)\rangle = \prod_{k,a=r,\theta}\frac{1}{2\pi}\int d\lambda_{ask} \times\lambda_{rsk}\, e^{-\frac{\lambda_{rsk}^2}{2}}\left(\rho\int_{-l/2}^{l/2} dr\cos\left[\chi(r,\{\lambda_{jsk}\}) - \theta\right]\right)^m, \tag{18}$$

where

$$\chi(r,\{\lambda_{jsk}\}) = \sum_k \sqrt{\frac{\left\langle|\hat{\phi}_{s,k}|^2\right\rangle}{L}}\lambda_{rsk}\sin(kr + \lambda_{\theta sk}), \tag{19}$$

$$\langle|\hat{\phi}_{s,k}|^2\rangle = \frac{\pi}{2|k|K_s}\frac{\sin^2(c_s|k|t) + \alpha_k^2\cos^2(c_s|k|t)}{\alpha_k}, \quad (k \neq 0),$$

$$\left\langle\phi_{s,0}^2\right\rangle_t = \frac{1}{2\rho\eta} + \left(\frac{c_s\pi t}{K_s}\right)^2\frac{\eta\rho}{2}, \quad (k = 0), \tag{20}$$

with $\alpha_k = \frac{|k|K_s}{\pi\rho\eta}$. The integration over λ_{rsk} and $\lambda_{\theta sk}$ in equation (18) extends from 0 to ∞ and from $-\pi$ to π, respectively.

Comparing the expression in equation (18) and the implicit definition of a distribution function in equation (2), it is easy to identify the distribution function as

$$P_l^{\theta}(\alpha) = \prod_k \int_{-\pi}^{\pi} \frac{\mathrm{d}\lambda_{\theta sk}}{2\pi} \int_0^{\infty} \lambda_{rsk}\, \mathrm{e}^{-\lambda_{rsk}^2/2}\, \mathrm{d}\lambda_{rsk}\, \delta\left(\alpha - \rho \int_{-l/2}^{l/2} \mathrm{d}r \cos\left[\chi(r, \{\lambda_{jsk}\}) - \theta\right]\right). \tag{21}$$

This function can be numerically evaluated through the Monte Carlo method with weight $\lambda_{rsk}\, \mathrm{e}^{-\lambda_{rsk}^2/2}$ for λ_{rsk} and equal unity weight for $\lambda_{\theta sk}$.

While we have assumed that the chemical potentials of spin-up and spin-down atoms are the same in the absence of interactions by going to the rotating frame, it is easy to obtain the expression for distribution functions in the laboratory frame. The energy difference E between spin-up and spin-down atoms results in the rotation of the spin in the x–y-plane at a constant angular velocity E. Therefore, the distribution in the laboratory frame is obtained by replacing $\theta \to \theta + Et$ in equation (21).

In this section, we have focused on the distribution function of spins in the x–y-plane, but it is also possible to obtain the distribution function of the z component of the spin, and we present the result in appendix (A.2).

4.2.4. Joint distribution function. From the expression for the spin operators in equation (9), we observe that the spin operators for the x and y directions commute in the low-energy description. This is because spin operators in the Tomonaga–Luttinger theory are coarse-grained over $\sim\rho\xi_{\mathrm{s}}$ particles, and since for weak interactions $\rho\xi_{\mathrm{s}} \gg 1$, the uncertainty of measurements coming from non-commutativity of $\hat{S}_l^x$ and $\hat{S}_l^y$ becomes suppressed. The possibility of simultaneous measurements of spin x and y operators implies the existence of joint distribution functions $P_l^{x,y}(\alpha, \beta)$, where $P_l^{x,y}(\alpha, \beta)\, \mathrm{d}\alpha\, \mathrm{d}\beta$ is the probability that the simultaneous measurements of $\hat{S}_l^x$ and S_l^y give values between α and $\alpha + \mathrm{d}\alpha$ and β and $\beta + \mathrm{d}\beta$, respectively. Here we provide the expression for $P_l^{x,y}(\alpha, \beta)$ and prove that this is indeed the unique solution.

The joint distribution function $P_l^{x,y}(\alpha, \beta)$ is given by the following expression,

$$P_l^{x,y}(\alpha, \beta) = \prod_k \int_{-\pi}^{\pi} \frac{\mathrm{d}\lambda_{\theta sk}}{2\pi} \int_0^{\infty} \lambda_{rsk}\, \mathrm{e}^{-\lambda_{rsk}^2/2}\, \mathrm{d}\lambda_{rsk}\, \delta\left(\alpha + \mathrm{i}\beta - \rho \int_{-l/2}^{l/2} \mathrm{d}r\, \mathrm{e}^{\mathrm{i}\chi(r, \{\lambda_{jsk}\})}\right), \tag{22}$$

where the expression for $\chi(r, \{\lambda_{jsk}\})$ is given in equation (19). To prove it, we first show that equation (22) reproduces the distribution function $P_l^{\theta}(\alpha)$ in equation (21) for all θ. Then, we show that a function with this property is unique, and therefore the expression in equation (21) is necessarily the joint distribution function.

Given a joint distribution function $P_l^{x,y}(\alpha, \beta)$, we can determine the distribution function $P_l^{\theta}(\gamma)$ of a spin pointing in the direction $(\cos\theta, \sin\theta, 0)$. Consider the spin $\vec{S}$ in the x–y-plane with $\vec{S} = (\alpha, \beta, 0)$ whose probability distribution is given by $P_l^{x,y}(\alpha, \beta)$. The projection of the spin $\vec{S}$ onto the axis pointing in the direction $(\cos\theta, \sin\theta, 0)$ is given by $|S|\cos(\phi - \theta)$, where $|S| = \sqrt{\alpha^2 + \beta^2}$ is the magnitude of spin and ϕ is the angle $\mathrm{Arg}(\alpha + \mathrm{i}\beta)$. After a simple algebra, we find that $|S|\cos(\phi - \theta) = \alpha\cos\theta + \beta\sin\theta$. Then, given a spin $\vec{S} = (\alpha, \beta, 0)$, if one measures the spin along the direction $(\cos\theta, \sin\theta, 0)$, the measurement result gives γ if and only if

$\gamma = \alpha\cos\theta + \beta\sin\theta$. From this consideration, the probability distribution that the measurement along the direction $(\cos\theta, \sin\theta, 0)$ gives the value γ is given by

$$P_l^{\theta}(\gamma) = \int \mathrm{d}\alpha\,\mathrm{d}\beta\, P_l^{x,y}(\alpha,\beta)\delta(\gamma - \alpha\cos\theta - \beta\sin\theta). \tag{23}$$

Now, if we plug the expression of equation (22) into equation (23), we see that $P_l^{\theta}(\gamma)$ agrees with equation (21) for all θ.

Now we prove the uniqueness of a function with the above property, i.e. a function that reproduces equation (21) through the relation (23). Suppose one has another distribution $\tilde{P}_l^{x,y}(\alpha,\beta)$ that satisfies equation (23) for all θ. We define $Q(\alpha,\beta) = P_l^{x,y}(\alpha,\beta) - \tilde{P}_l^{x,y}(\alpha,\beta)$. Our goal is to show that $Q(\alpha,\beta)$ must be equal to zero. By definition, we have the equality

$$0 = \int \mathrm{d}\alpha\,\mathrm{d}\beta\, Q(\alpha,\beta)\delta(\gamma - \alpha\cos\theta - \beta\sin\theta), \tag{24}$$

for all θ and γ. If we take the Fourier transform of both sides of equation (24) in terms of γ, we obtain

$$0 = \int \mathrm{d}\gamma \int \mathrm{d}\alpha\,\mathrm{d}\beta\, Q(\alpha,\beta)\delta(\gamma - \alpha\cos\theta - \beta\sin\theta)\mathrm{e}^{\mathrm{i}w\gamma} = \int \mathrm{d}\vec{\alpha}\, Q(\vec{\alpha})\mathrm{e}^{\mathrm{i}\vec{w}\cdot\vec{\alpha}}.$$

In the last line, we defined $\vec{w} = w(\cos\theta, \sin\theta)$ and $\vec{\alpha} = (\alpha,\beta)$. Note that this equation holds for any $\vec{w}$. Then this last expression is just like (2D) Fourier transform of Q. By taking the inverse Fourier transform of the last expression in terms of $\vec{w}$, we find

$$0 = \int_{-\infty}^{\infty} \mathrm{d}\vec{w} \int \mathrm{d}\vec{\alpha}\, Q(\vec{\alpha})\mathrm{e}^{\mathrm{i}\vec{w}\cdot(\vec{\alpha}-\vec{\alpha'})} Q(\vec{\alpha'}),$$

thereby proving the uniqueness of the joint distribution $P_l^{x,y}(\alpha,\beta)$.

From the joint distribution function in equation (22), one can also obtain other distributions, such as the distribution $P_l^{\perp}(\gamma)$ of the square of the transverse spin magnitude, $(S_l^{\perp}(t))^2$, which is given by

$$\begin{aligned} P_l^{\perp}(\gamma) &= \int_{-\infty}^{\infty} \mathrm{d}\alpha\,\mathrm{d}\beta\, P_l^{x,y}(\alpha,\beta)\delta\left(\gamma - \alpha^2 - \beta^2\right) \\ &= \prod_k \int_{-\pi}^{\pi} \frac{\mathrm{d}\lambda_{\theta sk}}{2\pi} \int_0^{\infty} \lambda_{rsk}\,\mathrm{e}^{-\lambda_{rsk}^2/2}\,\mathrm{d}\lambda_{rsk}\,\delta\left(\gamma - \left|\rho\int_{-l/2}^{l/2} \mathrm{d}r\mathrm{e}^{\mathrm{i}\chi(r,\{\lambda_{jsk}\})}\right|^2\right). \end{aligned} \tag{25}$$

4.2.5. Interpretation of the distribution dynamics. The form of the distribution function in equation (22) encapsulates the interpretation in terms of dynamics originating from spin waves explained in section 2. Here $\mathrm{e}^{\mathrm{i}\chi(r,\{t_{jsk}\})}$ represents the spin direction at the coordinate r, where the x–y-plane of the spin component is taken to be a complex plane. Then equation (22) suggests that for a given instance of the set $\{\lambda_{jsk}\}$, $(S_l^x + \mathrm{i}S_l^y)$ is simply the sum of the local spin directions $\mathrm{e}^{\mathrm{i}\chi(r,\{\lambda_{jsk}\})}$ over the integration length l. The local spin direction at position r is determined by the phase $\chi(r,\{t_{jsk}\})$, which receives contributions from each spin wave of momentum k with strength $A_k(t) = \lambda_{rsk}\sqrt{\langle|\hat{\phi}_{\mathrm{s},k}(t)|^2\rangle}$. Spin waves with momenta k rotate the spins as $\sin(kr + \lambda_{\theta sk})$

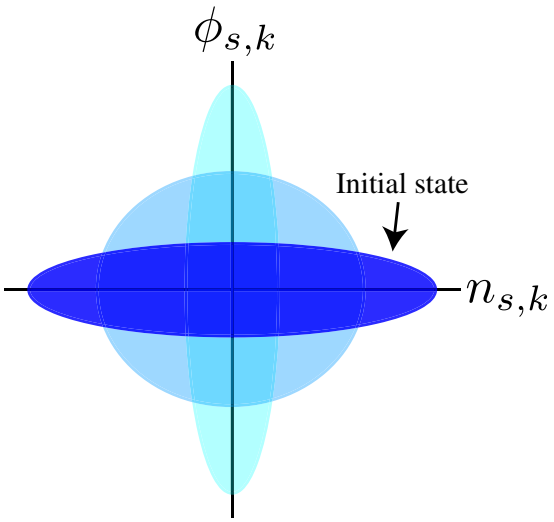

Figure 6. The illustration of the dynamics for each harmonic oscillator mode, described by the Hamiltonian equation (8). The initial state contains a large fluctuation of density difference $\hat{n}_{s,k}$ given by $\langle \hat{n}_{s,k}\hat{n}_{s,-k}\rangle = \eta\rho/2$ (see equation (10)), and its conjugate variable, the phase difference $\hat{\phi}_{s,k}$, has a small fluctuation. In the subsequent dynamics, such a squeezed state evolves and energy oscillates between the fluctuations of the density difference and phase difference.

(see the expression of $\chi(r, \{\lambda_{jsk}\})$ in equation (19)). The rotation strength $A_k(t) \propto \lambda_{rsk}$ has the distribution $\lambda_{rsk}\, e^{-\lambda_{rsk}^2/2}$, which represents the quantum fluctuation of the spins. On the other hand, $\lambda_{\theta sk}$ is distributed uniformly between $-\pi$ and π.

The dynamics of phase fluctuations $\langle|\hat{\phi}_{s,k}(t)|^2\rangle$ can, in fact, be easily understood by considering the Hamiltonian given by equation (8) as a harmonic oscillator for each k (figure 6). We first note that the initial state has a large fluctuation of density $\hat{n}_{s,k}$ because the initial $\pi/2$ pulse prepares the state in the (almost) eigenstate of $S^x = \rho\cos(\hat{\phi}_{s,k})$ with a small fluctuation of $\hat{\phi}_{s,k}$, the conjugate variable of $\hat{n}_{s,k}$. The fluctuation of $\hat{n}_{s,k}$ is given by $\langle \hat{n}_{s,k}\hat{n}_{s,-k}\rangle = \eta\rho/2$ (see equation (10)). Because of this large fluctuation in the density, almost all the energy of the initial state is stored in the interaction term $|n_{s,k}|^2$ in equation (8). Therefore, the total energy of each harmonic oscillator can be estimated as $\frac{\pi c_s \rho\eta}{4K_s}$. During the dynamics dictated by the harmonic oscillator Hamiltonian, this energy oscillates between the density fluctuations and phase fluctuations in a sinusoidal fashion, see figure 6. In the dephased limit of the dynamics, approximately equal energy of the system is distributed to the phase and density fluctuations, and from the conservation of energy, we conclude that the characteristic magnitude of phase fluctuation is given by $\langle|\phi_{s,k}(t)|^2\rangle \sim \frac{\pi^2\rho\eta}{4K_s^2k^2}$. Such $1/k^2$ dependence of $\langle|\hat{\phi}_{s,k}(t)|^2\rangle$ agrees with the more rigorous result in equation (20). Therefore the spin fluctuations dominantly come from spin waves with long wavelengths, as we have stated in section 2. Moreover, the weak dependence of spin dynamics on high momenta contributions justifies the use of the Tomonaga–Luttinger theory for describing the dynamics. We will more carefully analyze the dependence of distributions on the high momentum cutoff in section 4.4.

From the simple argument above, it is also clear that the spin fluctuations coming from spin waves with momenta k have the time scales associated with the harmonic oscillators

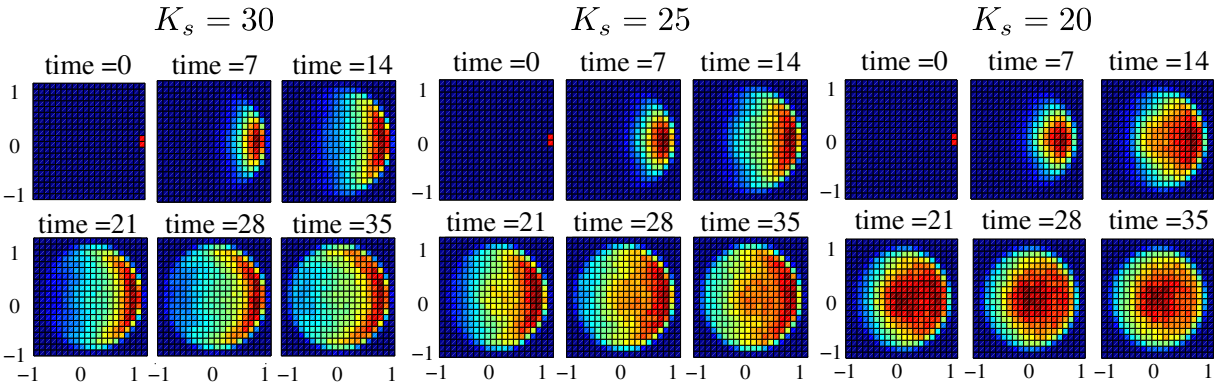

Figure 7. The dynamics of the joint distributions for $L/\xi_s = 200$, $\xi_s = 40$ and various spin Luttinger parameters $K_s = 30$, 25 and 20. Here axes are scaled such that the maximum values of α and β are 1. A smaller value of K_s enhances the spin fluctuations, leading to stronger diffusion and decay. Time is measured in units of ξ_s/c_s.

given by $\frac{1}{|k|c_s}$. Again, this rough argument agrees with the more rigorous result presented in equation (20). Therefore, the fast dynamics is dominated by spin waves with high momenta, and slow dynamics is dominated by low momenta. These considerations lead to the illustrative picture of figure 2. Furthermore, this implies that the dynamics of the magnitude of spin $(\hat{S}_l^{\perp})^2$ reaches a steady state around the time $\frac{l}{4c_s}$ since spin waves with wavelength longer than l do not affect the magnitude. This should be contrasted with the evolution of the x component of spin, which, in principle, keeps evolving until the time scale of $\sim\frac{L}{4c_s}$ (see figure 4).

The strength of interactions and correlations is associated with the Luttinger parameter, K_s. K_s influences the spin fluctuations $\langle|\phi_{s,k}(t)|^2\rangle$ at all wavelengths, and $\langle|\phi_{s,k}(t)|^2\rangle$ depends on K_s as $1/K_s^2$ for a fixed density. As was expected, in the limit of the weak interaction corresponding to large K_s, the amplitude of spin fluctuation decreases. In figure 7, we have plotted the time evolution of the joint distributions for $L/\xi_s = 200$, $l/\xi_s = 40$ and $K_s = 20$, 25 and 30. For larger K_s, we see that the spin fluctuations get suppressed quickly.

4.3. Dynamics of the expectation value of the magnitude of spin $\langle(\hat{S}_l^{\perp}(t))^2\rangle$

In order to illustrate the dynamics of the Ramsey sequence further, it is helpful to study the dynamics of the expectation value of the squared transverse magnitude, given by $\langle(\hat{S}_l^{\perp}(t))^2\rangle$.

In figure 8, we plot the evolution of $\sqrt{\langle(\hat{S}_l^{\perp}(t))^2\rangle}$ with $K_s = 20$, $L/\xi_s = 200$ and $l/\xi_s = 20$, 30 and 40 . We also plotted $\langle\hat{S}_l^x(t)\rangle$ along with $\sqrt{\langle(\hat{S}_l^{\perp}(t))^2\rangle}$ with the same parameters. It is easy to verify that $\langle S_l^x(t)\rangle$ is independent of integration length l [67]. As we have discussed in the previous section, $\sqrt{\langle(\hat{S}_l^{\perp}(t))^2\rangle}$ reaches steady states at the time scale of $\frac{l}{4c_s}$ with finite values, while $\langle\hat{S}_l^x(t)\rangle$ keeps decaying for a much longer time.

It is interesting to ask if the long time limit of $\sqrt{\langle(\hat{S}_l^{\perp}(t))^2\rangle}$ for sufficiently large integration length l attains the value that corresponds to the one expected from the randomization of spin patches of size ξ_s. At low energies, spins within the length $\sim\xi_s$ are aligned in the same direction,

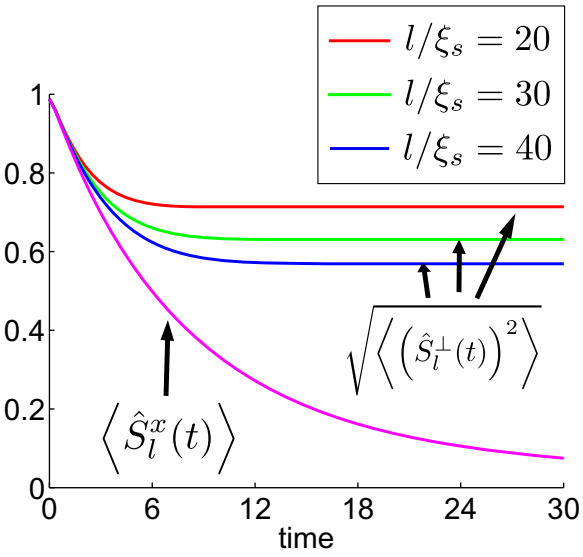

Figure 8. The dynamics of the average value of the magnitude of spins, $\sqrt{\langle(\hat{S}_l^{\perp}(t))^2\rangle}$, and the average of the x component of spins $\langle \hat{S}_l^x(t)\rangle$. Here the y-axis is scaled such that the initial values take the maximum value of 1. Here we took $L/\xi_s = 200$, $K_s = 20$ and the integration lengths $l/\xi_s = 20, 30, 40$. The magnitude of spins decays only due to the spin waves with wavelengths shorter than the integration length l, and the decay of the magnitude stops around the time scale of $\sim\frac{l}{4c_s}$. On the other hand, all spin waves contribute to the evolution of the x component of magnetization, which keeps decaying [67].

but spin waves can randomize the direction of the spin for each of l/ξ_s patches. Since the magnitude of spin within ξ_s is $\xi_s\rho$, if the patches are completely randomized, the result of the random walk predicts that $\sqrt{\langle(\hat{S}_l^{\perp})^2\rangle} \sim (\xi_s\rho)^2(l/\xi_s)$. We will see below that, due to the properties of correlations in 1D, the integrated magnitude of spin $\sqrt{\langle(\hat{S}_l^{\perp})^2\rangle}$ never attains this form, albeit a similar expression is obtained (see equation (26)). Moreover, we identify the integration length $\tilde{l}$ that separates the 'spin diffusion regime' and the 'spin decay regime' by finding the decaying length scale for $\sqrt{\langle(\hat{S}_l^{\perp})^2\rangle}$.

The results for the long time limit of $\langle(\hat{S}_l^{\perp}(t))^2\rangle$ can be analytically computed. Following similar steps leading to equation (17), we find that

$$\langle(\hat{S}_l^{\perp}(t))^2\rangle = \left\langle \left| \int \mathrm{d}r\rho\, \mathrm{e}^{\mathrm{i}\phi(s,r)} \right|^2 \right\rangle$$
$$= \prod_{i=1}^{2} \int_{-l/2}^{l/2} \rho\, \mathrm{d}r_i \exp\left(-\frac{1}{2} \sum_{k\neq 0} \xi_{\mathrm{s},k}^{\{r_i\}} (\xi_{\mathrm{s},k}^{\{,r_i\}})^* \right).$$

Here $\xi_{s,k}^{\{r_i\}} = |C_{s,k}|(e^{ikr_1} - e^{ikr_2})$. We introduce dimensionless variables $r_i' = r_i/l$, $k' = kl$ and the integration over k in the exponent can be carried out as

$$\int dk' \frac{L}{2\pi l} \xi_{s,k'}^{\{r_i'\}} \left(\xi_{s,k'}^{\{,r_i'\}}\right)^* = \frac{2}{\pi} \int_{k'_{min}}^{k'_c} dk' \left(\frac{1}{\rho\eta l} \cos^2(|k|c_s t) + \frac{\pi^2 \rho \eta l}{k'^2 K_s^2} \sin^2(|k|c_s t)\right) \sin^2\left(\frac{r_1' - r_2'}{2}|k'|\right)$$

$$\approx \frac{k'_c}{2\rho\pi l\eta} + \frac{\pi\eta\rho l}{2K_s}|r_1' - r_2'| \int_0^\infty dy \frac{\sin^2(y)}{y^2}.$$

In the second line, we approximated $\cos^2(|k|c_s t) \approx \sin^2(|k|c_s t) \approx 1/2$, which is appropriate for a long time. In the last line, we extended the upper limit of the integration for the second term to ∞ and the lower limit to 0. The former is justified because we know that the high momentum contribution is suppressed by $1/k^2$, and the latter is justified because we also know that low momenta excitations with wavelengths larger than l do not affect $\hat{S}_l^\perp$. Since $\int_0^\infty dy \frac{\sin^2(y)}{y^2} = \pi/2$, we find that, in the long time limit,

$$\langle(\hat{S}_l^\perp(t=\infty))^2\rangle / \langle(\hat{S}_l^\perp(t\approx 0))^2\rangle = 2\left\{\frac{1}{l_0} - \left(\frac{1}{l_0}\right)^2 (1 - \exp(-l_0))\right\}, \tag{26}$$

where we have expressed the result as a ratio of the asymptotic value to the value at the shortest time scale of the theory given by $t \sim 1/\mu$. Note that $l_0 = \frac{\pi^2\eta\rho l}{8K_s^2}$ is the dimensionless integration length that controls the value of $\langle(\hat{S}_l^\perp)^2\rangle$ in the long time limit. As soon as l_0 becomes larger than 1, the long time value of $\langle(\hat{S}_l^\perp)^2\rangle$ quickly approaches the long integration limit, $\propto 2\{\frac{1}{l_0} - (\frac{1}{l_0})^2\}$. Therefore, $l_0 \approx 1$ separates the 'spin diffusion regime' and the 'spin decay regime'.

The intuition behind the expression for l_0 can be explained through the following heuristic argument. The system enters the spin decay regime when the spins within the integration length l rotate by 2π across l. The difference in angle between the spins at $r = 0$ and $r = l$ in the long time limit is roughly given by $\Delta\chi = \frac{1}{\sqrt{L}} \sum_k \lambda_{rsk} \sqrt{\langle|\hat{\phi}_{s,k}|^2\rangle_{mean}} \sin(kl)$, where $\langle|\hat{\phi}_{s,k}|^2\rangle_{mean}$ is the characteristic magnitude of $\langle|\hat{\phi}_{s,k}(t)|^2\rangle$ in equation (20), which is given by half of the maximum magnitude of $\langle|\hat{\phi}_{s,k}(t)|^2\rangle$. Now the expectation of magnitude $\langle(\Delta\chi)^2\rangle$ over the quantum fluctuations represented by λ_{rsk} can be computed, and it yields $\langle(\Delta\chi)^2\rangle \approx \frac{\pi^2\eta\rho l}{4K_s^2}$. When $\sqrt{\langle(\Delta\chi)^2\rangle}$ becomes of the order of 1, the system enters the spin decay regime. This estimate gives the boundary between the two regimes $l_0 = \frac{\pi^2\eta\rho l}{8K_s^2} \approx 1$ apart from an unimportant numerical factor.

It is notable that equation (26) approaches the random walk behavior $\propto (\xi_s\rho)^2(l/\xi_s)$ very slowly, i.e. in an algebraic fashion. Therefore, even in the steady state, the system retains a strong correlation among spins. Moreover, equation (26) in the limit of $l_0 \to \infty$ is not just the random walk value, but is proportional to K_s, which measures the strength of fluctuations.

The calculation above shows that the spin diffusion regime and the spin decay regime are separated at the integration length scale of $\tilde{l} \approx \frac{8K_s^2}{\pi^2\eta\rho}$. This length scale is nothing but the correlation length of spins in the long time limit. Calculation of the spin correlation length, for example, between $S^x(r)$ and $\hat{S}^x(r')$, can be performed similarly to the calculation of $\langle(\hat{S}_l^\perp)^2\rangle$.

The result in the long time limit is

$$\langle \hat{S}^x(r)\hat{S}^x(r')\rangle \approx C\frac{\rho^2}{2}\mathrm{e}^{-|r-r'|/\tilde{l}}, \tag{27}$$

where $C = \mathrm{e}^{-k_c/(4\pi\rho\eta)}$ is a small reduction of the spins due to the contributions from the high-energy sector. Thus, one expects qualitatively different behavior of distribution functions for integration lengths $l < \tilde{l}$ and $l > \tilde{l}$.

4.4. Momentum cutoff dependence

The description of dynamics presented above uses the low-energy effective theory. In order to confirm the self-consistency of our approach, we check that the distributions of spins are not strongly affected by high-energy physics, i.e. they weakly depend on the high momentum cutoff. We have seen an indication that this is indeed the case through the weak fluctuations of phases for large k, $\langle|\hat{\phi}_{s,k}|\rangle \propto 1/k^2$, in section 4.2.5.

First of all, we analyze the high momentum cutoff $k_c \sim 2\pi/\xi_s$ dependence of the average value of $\hat{S}^x_l$. From the discussion in section 4.2, it is straightforward to obtain that (here we ignore the $k = 0$ contribution)

$$\begin{aligned}
\langle \hat{S}^x_l\rangle &= \int_{-l/2}^{l/2}\frac{\rho}{2}\mathrm{d}x\left\langle \mathrm{e}^{\mathrm{i}\phi(x)}+\mathrm{e}^{-\mathrm{i}\phi(x)}\right\rangle = \rho l\exp\left(-\frac{1}{2}\sum_{k\neq 0}|C_{s,k}|^2\right),\\
\sum_{k\neq 0}|C_{s,k}|^2 &= \int_{-k_c}^{k_c}\mathrm{d}k\left(\frac{\cos^2(|k|c_s t)}{4\pi\rho\eta}+\frac{\pi\rho\eta}{4k^2K_s^2}\sin^2(|k|c_s t)\right)\\
&\approx \frac{k_c}{2\pi\rho\eta}+\frac{\rho c_s t\eta}{(2K_s/\pi)^2},
\end{aligned} \tag{28}$$

where in the last line, we took the long time limit $t \gg \xi_s/c_s$ [67]. In this limit, only the first term in equation (28) depends on the cutoff k_c, and moreover, the cutoff dependence is independent of time. The effect is to reduce the value of $\langle \hat{S}^x_l\rangle$ through the multiplication of a number close to one in the weakly interacting limit. For example, if we take $k_c = 2\pi/\xi_c$, then the cutoff-dependent term reduces the value by multiplying $\exp(-\frac{k_c}{4\pi\rho\eta}) \approx \mathrm{e}^{-1/(4K_s)} \approx 1$.

In a similar fashion, higher moments of spin operators can be shown to have a weak dependence on the cutoff momentum k_c, as long as the integration length is much larger than the healing length, $l/\xi_s \gg 1$. In this limit, m moments of, for example, $\hat{S}^x_l$ are reduced by $\exp(-m\frac{k_c}{4\pi\rho\eta})$. Therefore, the full distribution function is simply reduced by the multiplication of a number close to one, $\exp(-\frac{k_c}{4\pi\rho\eta}) \approx \mathrm{e}^{-1/(4K_s)} \approx 1$, in the weakly interacting regime. This gives the self-consistency check of our results in section 4.2.

5. Dynamics of full distribution functions in the presence of mixing between spin and charge degrees of freedom

In this section, we extend the analysis in section 4 to a more general case in which spin and charge degrees of freedom mix. We will see that the distribution functions even for this more

general case have essentially the same structure as in equation (21), and are described by spin waves with fluctuations whose amplitude is determined by the fluctuations of phase $\langle|\hat{\phi}_{s,k}|^2\rangle$. One important difference from the decoupling case is the dependence of spin distributions on the initial temperature of the system. The thermal excitations are present in the charge degrees of freedom in the initial state, and such thermal fluctuations increase the value of $\langle|\hat{\phi}_{s,k}|^2\rangle$ through the coupling between spin and charge during the evolution.

5.1. The Hamiltonian and the initial state

In a generic system of two-component bosons in 1D, spin and charge degrees of freedom couple through the mixing Hamiltonian in equation (7). Yet, the Hamiltonian in equation (4) is still quadratic and it can be diagonalized. We define new operators $\hat{\phi}_1, \hat{\phi}_2, \hat{n}_1, \hat{n}_2$ by

$$\begin{pmatrix}\hat{\phi}_1\\ \hat{\phi}_2\end{pmatrix} = \begin{pmatrix}\cos\kappa & \sin\kappa\\ -\sin\kappa & \cos\kappa\end{pmatrix}\begin{pmatrix}\sqrt{s_c}\hat{\phi}_c\\ \hat{\phi}_s\end{pmatrix}, \tag{29}$$

$$\begin{pmatrix}\hat{n}_1\\ \hat{n}_2\end{pmatrix} = \begin{pmatrix}\cos\kappa & \sin\kappa\\ -\sin\kappa & \cos\kappa\end{pmatrix}\begin{pmatrix}\frac{1}{\sqrt{s_c}}\hat{n}_c\\ \hat{n}_s\end{pmatrix}. \tag{30}$$

The mixing angle κ and the scaling parameter s_c are chosen so that the Hamiltonian is written in the following diagonal form:

$$\begin{aligned} H &= H_1 + H_2,\\ H_1 &= \int_{-L/2}^{L/2} \mathrm{d}r \frac{\rho}{2m_1}(\nabla\hat{\phi}_1(r))^2 + g_1(\hat{n}_1)^2,\\ H_2 &= \int_{-L/2}^{L/2} \mathrm{d}r \frac{\rho}{2m_2}(\nabla\hat{\phi}_2)^2 + g_2(\hat{n}_2)^2. \end{aligned} \tag{31}$$

Explicitly, κ and s_c are given by

$$s_c = \frac{\frac{g_{mix}\rho}{2m_c} + g_s g^{\phi}_{mix}}{g_c g^{\phi}_{mix} + \frac{g_{mix}\rho}{2m_s}}, \qquad \tan\kappa = \frac{-\kappa_0 \pm \sqrt{\kappa_0^2+4}}{2},$$

$$\kappa_0 = \frac{s_c g_c - g_s}{\sqrt{s_c} g_{mix}} = \frac{\frac{\rho}{2m_c} - s_c\frac{\rho}{2m_s}}{g^{\phi}_{mix}\sqrt{s_c}},$$

where $\pm$ in the expression of $\tan\kappa$ is $+$ when $\kappa_0 > 0$ and $-$ when $\kappa_0 < 0$. We defined κ such that $\kappa = 0$ corresponds to decoupling of charge and spin, i.e. to $g_{mix} = 0$ and $g^{\phi}_{mix} = 0$ in

equation (7). The parameters g_1, g_2, $\frac{\rho}{2m_1}$ and $\frac{\rho}{2m_2}$ are given by

$$g_1 = s_c g_c + \sqrt{s_c}\tan\kappa\, g_{mix},$$
$$g_2 = g_s - \sqrt{s_c}\tan\kappa\, g_{mix},$$
$$\frac{\rho}{2m_1} = \frac{\rho}{2m_c s_c} + \tan\kappa\,\frac{g^{\phi}_{mix}}{\sqrt{s_c}},$$
$$\frac{\rho}{2m_2} = \frac{\rho}{2m_s} - \tan\kappa\,\frac{g^{\phi}_{mix}}{\sqrt{s_c}}.$$

In the weakly interacting systems that we study in this paper, the Luttinger parameters K_i and sound velocities c_i are determined for each Hamiltonian H_i, $i = \uparrow, \downarrow, c, s, 1, 2$, through

$$K_i = \pi\sqrt{\frac{\rho}{2m_i g_i}}, \quad c_i = \sqrt{\frac{\rho g_i}{m_i}}. \tag{32}$$

At finite temperature, the state before the first $\pi/2$ pulse contains excitations, and these excitations are carried over to the charge degrees of freedom after the pulse. The pulse only acts on the spin degrees of freedom, and the local sum density of spin up and down is left untouched as long as the pulse is applied in a short time compared to the inverse of typical excitation energies, $\beta = 1/(k_B T)$. In other words, the local density fluctuation of spin up, $\hat{n}_\uparrow(r)$, before the $\pi/2$ pulse is converted to the sum of the local density fluctuation of spin up and spin down, $\hat{n}_\uparrow(r) + \hat{n}_\downarrow(r)$ after the $\pi/2$ pulse. In this strong pulse limit, then, the distribution of $\hat{n}_\uparrow(r)$ before the $\pi/2$ pulse is the same as the distribution of $\hat{n}_\uparrow(r) + \hat{n}_\downarrow(r)$ after the $\pi/2$ pulse.

The distribution of the local density for spin-up atoms before the $\pi/2$ pulse is determined by the density matrix for spin up given by $e^{-\beta H'_\uparrow}$, where in the weak interaction regime we have (see equation (4))

$$H'_\uparrow = \int_{-L/2}^{L/2} dr \left[\frac{2\rho}{2m_\uparrow}(\nabla\hat{\phi}_\uparrow(r))^2 + g_{\uparrow\uparrow}(\hat{n}_\uparrow(r))^2\right].$$

Then, the density matrix that produces the distribution of $\hat{n}_\uparrow(r) + \hat{n}_\downarrow(r)$ required above is given by $e^{-\beta H_{c\uparrow}}$ where

$$\begin{aligned} H_{\uparrow c} &= \int_{-L/2}^{L/2} dr \left[\frac{2\rho}{2m_\uparrow}\{(\nabla\hat{\phi}_\uparrow(r) + \nabla\hat{\phi}_\downarrow(r))/2\}^2 + g_{\uparrow\uparrow}(\hat{n}_\uparrow(r) + \hat{n}_\downarrow(r))^2\right] \\ &= \frac{c_{c\uparrow}}{2}\int_{-L/2}^{L/2} dr \left[\frac{K_{c\uparrow}}{\pi}(\nabla\hat{\phi}_c)^2 + \frac{\pi}{K_{c\uparrow}}\hat{n}_c^2\right], \end{aligned} \tag{33}$$

where $K_{c\uparrow} = \frac{\pi}{4}\sqrt{\frac{\rho}{m_\uparrow g_{\uparrow\uparrow}}}$ and $c_{c\uparrow} = \sqrt{\frac{2\rho g_{\uparrow\uparrow}}{m_\uparrow}}$.

The initial state for spins is determined by the $\pi/2$ pulse, and we obtained the state in equation (12). Then, the complete initial density matrix after the first $\pi/2$ pulse is given by

$$\hat{\rho}_0 = |\psi_0\rangle\langle\psi_0| \otimes e^{-\beta H_{c\uparrow}}/\mathrm{Tr}\left(e^{-\beta H_{c\uparrow}}\right). \tag{34}$$

This density matrix evolves in time as $\hat{\rho}(t) = e^{-itH}\hat{\rho}_0\, e^{itH}$. Since we assume that the preparation of the initial state is done through a strong, short pulse, the spin and charge degrees of freedom are not entangled in the initial state.

5.2. Time evolutions of operators

In order to calculate the distribution function of $\hat{S}_l^\theta$, we again start from the calculation of the mth moments, $\mathrm{Tr}(\hat{\rho}(t)(\hat{S}_l^\theta)^m)$. Evaluation of moments can be done through a similar technique to that used in section 4.2.

In the following, we describe convenient, time-dependent operators $\gamma_{\mathrm{s},k}(t)$ and $\gamma_{\mathrm{c},k}(t)$ used to evaluate spin operators such as $\mathrm{e}^{\mathrm{i}\hat{\phi}_{\mathrm{s},k}}$. The first operator resides in the spin sector and it is again the annihilation operator of the initial spin state such that $\mathrm{Tr}\,\gamma_{\mathrm{s},k}(0)\hat{\rho}_0 = 0$. This operator is given in equation (15), which is

$$\gamma_{\mathrm{s},k}(t) = \mathrm{e}^{-\mathrm{i}tH}\gamma_{\mathrm{s},k}(0)\mathrm{e}^{\mathrm{i}tH},$$

$$\begin{pmatrix}\gamma^\dagger_{\mathrm{s},-k}(0)\\ \gamma_{\mathrm{s},k}(0)\end{pmatrix} = \begin{pmatrix}\dfrac{1}{\sqrt{1-4|W_k|^2}} & \dfrac{-2W_k}{\sqrt{1-4|W_k|^2}}\\ \dfrac{-2W_k}{\sqrt{1-4|W_k|^2}} & \dfrac{1}{\sqrt{1-4|W_k|^2}}\end{pmatrix}\begin{pmatrix}b^\dagger_{\mathrm{s},-k}\\ b_{\mathrm{s},k}\end{pmatrix},$$

with $2W_k = \frac{1-\alpha_k}{1+\alpha_k}$ and $\alpha_k = \frac{|k|K_\mathrm{s}}{\pi\rho\eta}$ as before. The second operator is the operator of charge degrees of freedom, and it is given by

$$\gamma_{\mathrm{c},k}(t) = \mathrm{e}^{-\mathrm{i}tH}\gamma_{\mathrm{c},k}(0)\mathrm{e}^{\mathrm{i}tH},$$
$$\gamma_{\mathrm{c},k}(0) = b_{\mathrm{c}\uparrow,k},$$

where $b_{\mathrm{c}\uparrow,k}$ is an annihilation operator for the elementary excitations in $H_{\mathrm{c}\uparrow}$. Since $\gamma_{\mathrm{s},k}(t)$ and $\gamma_{\mathrm{c},k}(t)$ commute at $t = 0$, they commute at any time t. We will drop the time dependence of $\gamma_{a,k}(t)$ in the notation from now on.

From the expression of the initial density matrix $\hat{\rho}_0$ in equation (34), it is easy to check that the density matrix at time t given by $\hat{\rho}(t) = \mathrm{e}^{-\mathrm{i}tH}\hat{\rho}_0\,\mathrm{e}^{\mathrm{i}tH}$ can be written as the tensor product of the density matrix of operators $\gamma_{\mathrm{s},k}(t)$ and that of $\gamma_{\mathrm{c},k}(t)$. This is because $\hat{\rho}_0$ is a tensor product of the density matrices of $\gamma_{\mathrm{s},k}(t=0)$ and that of $\gamma_{\mathrm{c},k}(t=0)$. This structure of the density matrices at time t allows the independent evaluation of $\gamma_{\mathrm{s},k}(t)$ and $\gamma_{\mathrm{c},k}(t)$ operators, and it is advantageous to express spin operators in terms of these operators.

As we show in appendix B, we can write $\hat{\phi}_{\mathrm{s},k}$ in terms of $\gamma_{\mathrm{c},k}(t)$ and $\gamma_{\mathrm{s},k}(t)$ as follows:

$$\frac{1}{\sqrt{L}}\hat{\phi}_{\mathrm{s},k} = C^*_{\mathrm{s},k}\gamma^\dagger_{\mathrm{s},-k} + C_{\mathrm{s},k}\gamma_{\mathrm{s},k} + C^*_{\mathrm{c},k}\gamma^\dagger_{\mathrm{c},-k} + C_{\mathrm{c},k}\gamma_{\mathrm{c},k}, \tag{35}$$

where explicit expressions of $C_{\mathrm{s},k}$ and $C_{\mathrm{c},k}$ are given by

$$C_{\mathrm{s},k} = \mathrm{i}\sqrt{\frac{1}{2L\rho\eta}}\left(\{\cos^2\theta\cos(c_2|k|t) + \sin^2\theta\cos(c_1|k|t)\}\right.$$
$$\left.-\mathrm{i}\frac{K_\mathrm{s}}{\alpha_k}\left\{\frac{\cos^2\theta\sin(c_2|k|t)}{K_2} + \frac{\sin^2\theta\sin(c_1|k|t)}{K_1}\right\}\right),$$

$$C_{\mathrm{c},k} = \cos\theta\sin\theta\sqrt{\frac{\pi}{2L|k|s_\mathrm{c}\tilde{K}_{\mathrm{c}\uparrow}}}$$
$$\times\left(\mathrm{i}\{\cos(c_1|k|t) - \cos(c_2|k|t)\} - \tilde{K}_{\mathrm{c}\uparrow}\left\{\frac{\sin(c_2|k|t)}{K_2} - \frac{\sin(c_1|k|t)}{K_1}\right\}\right), \tag{36}$$

where $\tilde{K}_{\mathrm{c}\uparrow} = K_{\mathrm{c}\uparrow}/\sqrt{s_\mathrm{c}}$.

Using equation (35), we find an expression for $(\hat{S}_l^\theta)^m$ in terms of $\gamma_{a,k}$ with $a = s, c$ as follows:

$$(\hat{S}_l^\theta)^m = \prod_{i=1}^{m} \int_{-l/2}^{l/2} \mathrm{d}r_i \frac{\rho}{2} \sum_{\{s_i\}} \mathrm{e}^{\mathrm{i}\sum_{k\neq 0}(\xi^*_{\mathrm{s},k}\gamma^\dagger_{\mathrm{s},k}+\xi_{\mathrm{s},k}\gamma_{\mathrm{s},k})} \mathrm{e}^{\mathrm{i}\sum_{k\neq 0}(\xi^*_{\mathrm{c},k}\gamma^\dagger_{\mathrm{c},k}+\xi_{\mathrm{c},k}\gamma_{\mathrm{c},k})} \mathrm{e}^{\mathrm{i}(\sum_i s_i)\phi_{\mathrm{s},0}/\sqrt{L}} \mathrm{e}^{-\mathrm{i}(\sum_i s_i)\theta},$$

where $\xi_{a,k} = (\sum_i^m s_i \mathrm{e}^{\mathrm{i}r_i k})C_{a,k}$. In the following, we separately evaluate three contributions: the $k = 0$ component given by $\mathrm{e}^{\mathrm{i}(\sum_i s_i)\phi_{\mathrm{s},0}/\sqrt{L}}$; the charge component of $k \neq 0$ given by $\mathrm{e}^{\mathrm{i}\sum_{k\neq 0}(\xi^*_{\mathrm{c},k}\gamma^\dagger_{\mathrm{c},k}+\xi_{\mathrm{c},k}\gamma_{\mathrm{c},k})}$; and the spin component of $k \neq 0$ given by $\mathrm{e}^{\mathrm{i}\sum_{k\neq 0}(\xi^*_{\mathrm{s},k}\gamma^\dagger_{\mathrm{s},k}+\xi_{\mathrm{s},k}\gamma_{\mathrm{s},k})}$.

5.2.1. The $k = 0$ contribution. The initial state of the $k = 0$ spin sector in equation (12) as well as that of the charge sector in equation (33) have a Gaussian form so that calculation of the trace $\mathrm{Tr}\{\mathrm{e}^{\mathrm{i}(\sum_i s_i)\phi_{\mathrm{s},0}/\sqrt{L}}\hat{\rho}(t)\}$ is straightforward. We leave the details to appendix C, and the result is

$$\begin{aligned} \langle \mathrm{e}^{\mathrm{i}(\sum_i s_i)\phi_{\mathrm{s},0}/\sqrt{L}} \rangle &= \exp\left(-\left(\sum_i s_i\right)^2 \frac{\langle \phi^2_{\mathrm{s},0}\rangle_t}{2L} \right), \\ \langle \phi^2_{\mathrm{s},0}\rangle_t &= \frac{1}{2\rho\eta} + \left(\sin^2\theta \frac{\pi c_1}{K_1} + \cos^2\theta \frac{\pi c_2}{K_2}\right)^2 \frac{\rho\eta}{2} t^2 + \sin^2\theta\cos^2\theta \left(\frac{\pi c_1}{K_1} - \frac{\pi c_2}{K_2}\right)^2 \frac{\tilde{K}_{\mathrm{c}\uparrow}}{\pi c_{\mathrm{c}\uparrow}\beta} t^2. \end{aligned} \tag{37}$$

5.2.2. The $k \neq 0$ spin sector. This calculation is analogous to equation (17), and the result can be directly read off from equation (17) and it is

$$\langle \mathrm{e}^{\mathrm{i}\sum_{k\neq 0}(\xi^*_{\mathrm{s},k}\gamma^\dagger_{\mathrm{s},k}+\xi_{\mathrm{s},k}\gamma_{\mathrm{s},k})} \rangle = \exp\left(-\frac{1}{2} \sum_{k\neq 0} \xi^*_{\mathrm{s},k}\xi_{\mathrm{s},k} \right). \tag{38}$$

5.2.3. The $k \neq 0$ charge sector. We first rewrite the density matrix at time t as

$$\begin{aligned} \hat{\rho}_{\mathrm{c},k\neq 0}(t) &= \mathrm{e}^{-\mathrm{i}tH}\, \mathrm{e}^{-\beta c_{\mathrm{c}\uparrow}\sum_{k\neq 0}|k| b^\dagger_{\mathrm{c}\uparrow,k} b_{\mathrm{c}\uparrow,k}}\, \mathrm{e}^{\mathrm{i}tH}/\mathcal{N} \\ &= \mathrm{e}^{-\beta c_{\mathrm{c}\uparrow}\sum_{k\neq 0}|k|\gamma^\dagger_{\mathrm{c},k}(t)\gamma_{\mathrm{c},k}(t)}/\mathcal{N}, \end{aligned}$$

where $\mathcal{N}_\mathrm{c}$ is normalization given by $\mathcal{N}_\mathrm{c} = \mathrm{Tr}\, \mathrm{e}^{-\beta c_{\mathrm{c}\uparrow}\sum_{k\neq 0}|k|\gamma^\dagger_{\mathrm{c},k}(t)\gamma_{\mathrm{c},k}(t)} = \prod_{k\neq 0} -1/\lambda_k$ with $\lambda_k = \mathrm{e}^{-\beta c_{\mathrm{c}\uparrow}|k|} - 1$.

Then the trace of $(\hat{S}_l^\theta)^m$ for the $k \neq 0$ spin sector is

$$\langle \mathrm{e}^{\mathrm{i}\sum_{k\neq 0}(\xi^*_{\mathrm{c},k}\gamma^\dagger_{\mathrm{c},k}+\xi_{\mathrm{c},k}\gamma_{\mathrm{c},k})} \rangle = \prod_{k\neq 0} \mathrm{Tr}(\mathrm{e}^{\mathrm{i}(\xi^*_{\mathrm{c},k}\gamma^\dagger_{\mathrm{c},k}+\xi_{\mathrm{c},k}\gamma_{\mathrm{c},k})}\, \mathrm{e}^{-\beta|k|c_{\mathrm{c}\uparrow}\gamma^\dagger_{\mathrm{c},k}\gamma_{\mathrm{c},k}}) \Big/ \mathcal{N}. \tag{39}$$

We can evaluate this by taking the trace in the basis of normalized coherent states $|\alpha_k\rangle$ such that $\gamma_{\mathrm{c},k}|\alpha_k\rangle = \alpha_k|\alpha_k\rangle$. The use of the identity $1 = \frac{1}{\pi}\int \mathrm{d}^2\alpha_k |\alpha_k\rangle\langle\alpha_k|$ as well as of an important

equality $e^{va^\dagger a} = :e^{(e^v-1)a^\dagger a}:$ [18], where $:\mathcal{O}:$ is a normal ordering of $\mathcal{O}$, leads to

$$\begin{aligned}\langle e^{i\sum_{k\neq 0}(\xi^*_{c,k}\gamma^\dagger_{c,k}+\xi_{c,k}\gamma_{c,k})}\rangle &= \frac{1}{\mathcal{N}}\prod_{k\neq 0}\frac{1}{\pi}\int d^2\alpha_k\,\langle\alpha_k|\,e^{i(\xi^*_{c,k}\gamma^\dagger_{c,k}+\xi_{c,k}\gamma_{c,k})}\,e^{-\beta|k|c_{c\uparrow}\gamma^\dagger_{c,k}\gamma_{c,k}}\,|\alpha_k\rangle\\ &= \frac{1}{\mathcal{N}}\prod_{k\neq 0}\frac{1}{\pi}\int d^2\alpha_k\,e^{-1/2\xi^*_{c,k}\xi_{c,k}}\,\langle\alpha_k|\,e^{i\xi^*_{c,k}\alpha^*_k}\,e^{i\xi_{c,k}\gamma_{c,k}}:e^{\lambda_k\gamma^\dagger_{c,k}\gamma_{c,k}}:|\alpha_k\rangle\\ &= \prod_{k\neq 0}e^{-\frac{1}{2}\frac{1+e^{-\beta|k|c_{c\uparrow}}}{1-e^{-\beta|k|c_{c\uparrow}}}\xi^*_{c,k}\xi_{c,k}}.\end{aligned}$$

5.2.4. Full distribution function. We can summarize the results above as follows:

$$\begin{aligned}\left\langle(\hat{S}^\theta_l)^n\right\rangle = \sum_{\{s_i\}}\prod_{i=1}^m\int dr_i\frac{\rho}{2}\exp\left(-\frac{1}{2}\sum_{k\neq 0}\xi^*_{s,k}\xi_{s,k}\right)\exp\left(-\frac{1}{2}\sum_{k\neq 0}M_{c,k}\xi^*_{c,k}\xi_{c,k}\right)\\ \times\exp\left(-\frac{1}{2}\left(\sum_i s_i\right)^2\frac{\langle\phi^2_{s,0}\rangle_t}{L}\right)e^{-i(\sum_i s_i)\theta}\end{aligned}\tag{40}$$

Here, $M_{c,k} = \frac{1+e^{-\beta|k|c_{c\uparrow}}}{1-e^{-\beta|k|c_{c\uparrow}}}$. As before, we introduce the auxiliary variables to separate spatial integrations over r_i. We can combine $\xi^*_{s,k}\xi_{s,k}$ and $M_{c,k}\xi^*_{c,k}\xi_{c,k}$ so that we only need to introduce three sets of variables, $\lambda_{1,s,k}$, $\lambda_{2,s,k}$, λ_0, for the Hubbard–Stratonovich transformation. Summing over $\{s_i\}$ simplifies the result, leading to the following expression for the full distribution function:

$$P^\theta_l(\alpha) = \prod_k\int_{-\pi}^{\pi}\frac{d\lambda_{\theta sk}}{2\pi}\int_0^\infty\lambda_{rsk}\,e^{-\lambda^2_{rsk}/2}\,d\lambda_{rsk},\,\delta\left(\alpha-\rho\int_{-l/2}^{l/2}dr\,\cos[\chi(r,\{\lambda_{jsk}\})-\theta]\right),$$

$$\chi(r,\{\lambda_{jsk}\}) = \sum_k\sqrt{\frac{\langle|\hat{\phi}_{s,k}|^2\rangle}{L}}\lambda_{rsk}\sin(kr+\lambda_{\theta sk}),\tag{41}$$

$$\langle|\hat{\phi}_{s,k}|^2\rangle/L = |C_{s,k}|^2 + \frac{1+e^{-\beta|k|c_{c\uparrow}}}{1-e^{-\beta|k|c_{c\uparrow}}}|C_{c,k}|^2,\quad k\neq 0.$$

The last line can be confirmed by directly computing $\langle|\hat{\phi}_{s,k}|^2\rangle$ using the expression in equation (35). The expression for $\langle|\phi_{s,0}|^2\rangle$ is given by equation (37). As before, the joint distributions as well as the distributions of squared transverse magnitude can be obtained through the same procedure as that in section 4.2.4.

The spin distribution in the presence of mixing between spin and charge degrees of freedom resembles that in the absence of such mixing, and the only change is the additional contributions to phase fluctuations coming from the thermal excitations, represented by $\frac{1+e^{-\beta|k|c_{c\uparrow}}}{1-e^{-\beta|k|c_{c\uparrow}}}|C_{c,k}|^2$ in equation (41). $|C_{c,k}|$ is proportional to $\sin^2\kappa$ as one can see from equation (36). Thus, for weak coupling of $\kappa\sim 0$, the contribution is diminished by a factor of κ^2.

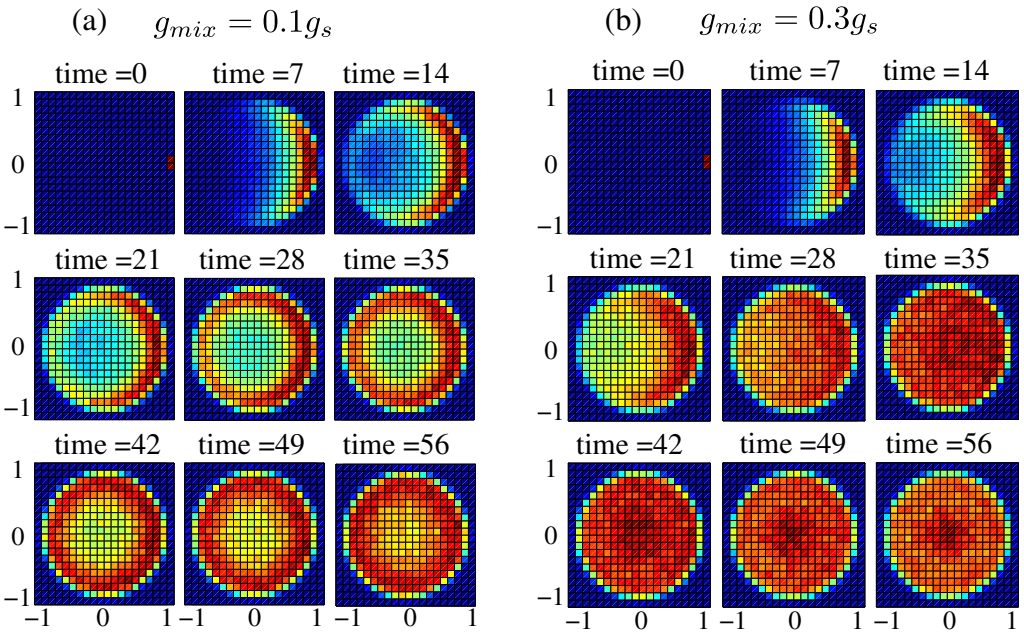

Figure 9. Time evolution of the joint distribution function $P^{x,y}(\alpha, \beta)$ for the system size $L/\xi_s = 400$, the spin Luttinger parameter $K_s = 20$ and the integration length $l/\xi_s = 20$ in the presence of mixing between the spin and charge modes. For (a), the interaction strength ratio is taken to be $g_c : g_s : g_{mix} = 1 : 1 : 0.1$, and for (b), $g_c : g_s : g_{mix} = 1 : 1 : 0.3$. Time is measured in units of ξ_s/c_s, where c_s is the spin sound wave velocity. Here, the axes are scaled such that the maximum values of α and β are 1. With increasing strength of mixing, the large initial temperature affects the spin dynamics at earlier time more strongly.

In the experiment by Widera *et al*, they used Rb^{87} in the presence of Feshbach resonance. They employed the theory which assumes the absence of mixing between spin and charge degrees of freedom to analyze the decay of the Ramsey fringes. The ratio of interaction strengths in their experiment can be roughly estimated as $g_c : g_s : g_{mix} \approx 3.66 : 0.34 : 0.06$, which leads to the value of $\kappa \approx 2 \times 10^{-2}$. Therefore, the thermal contributions are diminished by about four orders of magnitude and thus their assumption of decoupling between spin and charge is justified.

In figure 9, we have plotted the evolution of the joint distribution functions for different strengths of the coupling g_{mix} at a relatively large initial temperature $k_B T = 0.4 \times 2\pi c_{c\uparrow}/\xi_s$, where $2\pi c_{c\uparrow}/\xi_s$ is approximately the high-energy cutoff of the Tomonaga–Luttinger theory. Here we took the system size $L/\xi_s = 400$, the Luttinger parameter $K_s = 20$ and the integration length $l = 20\xi_s$. For figure 9(a), the ratio of interaction is taken to be $g_c : g_s : g_{mix} = 1 : 1 : 0.1$, and for figure 9(b), $g_c : g_s : g_{mix} = 1 : 1 : 0.3$. One can see that with increasing strength of mixing, the large initial temperature affects the spin dynamics at earlier time more strongly. For comparison, also see figure 4.

6. Interference of two 1D condensates

6.1. Dynamics of interference patterns

As we have described in section 2.2, the full distribution of interference patterns can be studied in exactly the same way as we have studied the full distribution of spins in previous sections. In the following, we more formally describe the dynamics of split condensates.

The low-energy effective Hamiltonian of two quasi-condensates after splitting is given by

$$\begin{aligned} H &= H_{\mathrm{L}} + H_{\mathrm{R}}, \\ H_{\mathrm{L}} &= \int_{-L/2}^{L/2} \mathrm{d}r \left[\frac{\rho_{\mathrm{L}}}{2m} (\nabla \hat{\phi}_{\mathrm{L}}(r))^2 + \frac{g}{2} (\hat{n}_{\mathrm{L}}(r))^2 \right], \\ H_{\mathrm{R}} &= \int_{-L/2}^{L/2} \mathrm{d}r \left[\frac{\rho_{\mathrm{R}}}{2m} (\nabla \hat{\phi}_{\mathrm{R}}(r))^2 + \frac{g}{2} (\hat{n}_{\mathrm{R}}(r))^2 \right], \end{aligned} \tag{42}$$

where we have assumed weakly interacting bosons with a possible density difference $\rho_{\mathrm{R}} - \rho_{\mathrm{L}} \neq 0$ between the two condensates. Here and in the following, we consider the rotating frame and ignore the chemical potential difference $g/2(\rho_{\mathrm{R}}^2 - \rho_{\mathrm{L}}^2)$ between the left and right condensates arising from interactions.

The interference pattern measures the phase difference $\hat{\phi}_{\mathrm{L}} - \hat{\phi}_{\mathrm{R}}$. We describe the system in terms of the 'spin' variables that are the difference of left and right condensates and 'charge' variables that are the sum of the two. Using the variables $\hat{\phi}_{\mathrm{s}} = \hat{\phi}_{\mathrm{R}} - \hat{\phi}_{\mathrm{L}}$, $\hat{\phi}_c = \hat{\phi}_{\mathrm{R}} + \hat{\phi}_{\mathrm{L}}$, $\hat{n}_{\mathrm{s}} = (\hat{n}_{\mathrm{R}} - \hat{n}_{\mathrm{L}})/2$ and $\hat{n}_{\mathrm{c}} = (\hat{n}_{\mathrm{R}} + \hat{n}_{\mathrm{L}})/2$, we find the Hamiltonian of the system to be

$$H = H_{\mathrm{s}} + H_{\mathrm{c}} + H_{\mathrm{int}}, \tag{43}$$

$$H_{\mathrm{s}} = \int \mathrm{d}x \left[\frac{\rho_{\mathrm{R}} + \rho_{\mathrm{L}}}{8m} (\partial_x \hat{\phi}_{\mathrm{s}})^2 + g \hat{n}_{\mathrm{s}}^2 \right], \tag{44}$$

$$H_{\mathrm{c}} = \int \mathrm{d}x \left[\frac{\rho_{\mathrm{R}} + \rho_{\mathrm{L}}}{8m} (\partial_x \hat{\phi}_{\mathrm{c}})^2 + g \hat{n}_{\mathrm{c}}^2 \right], \tag{45}$$

$$H_{\mathrm{int}} = \int \mathrm{d}x \left[\frac{\rho_{\mathrm{R}} - \rho_{\mathrm{L}}}{4m} \partial_x \hat{\phi}_{\mathrm{c}} \partial_x \hat{\phi}_{\mathrm{s}} \right]. \tag{46}$$

Therefore, when the splitting makes two identical quasi-condensates with equal density, 'spin' and 'charge' degrees of freedom decouple and we can use a simpler theory derived in section 4.2. On the other hand, when the splitting makes two condensates with unequal densities, the more general theory of section 5 needs to be employed. In any case, the full time evolution of the distributions of interference patterns can be obtained, which in principle can be compared with experiments.

It is notable that the mixing of the 'spin' and 'charge' degrees of freedom for a small density difference $\rho_{\mathrm{R}} - \rho_{\mathrm{L}}$ is not 'small', in the sense that the mixing angle κ defined in section 5 takes the maximum value $\pi/4$. The spin decoupling in the limit of $\rho_{\mathrm{R}} - \rho_{\mathrm{L}} \to 0$ is recovered not by taking $\kappa \to 0$, but rather, by taking the time at which the effect of the coupling takes place to infinity. This is most explicitly shown in equation (36) where the charge contributions of fluctuations go to zero as $c_1 \to c_2$, which is attained in the limit $\rho_{\mathrm{R}} - \rho_{\mathrm{L}} = 0$.

6.2. Interference patterns in equilibrium

The techniques for calculating the full distribution functions presented in previous sections are directly applicable also to obtaining a simple form of the full distribution functions of the interference patterns between two independent, thermal quasi-condensates. This problem has been previously analyzed in theory [68, 69] as well as in experiments [14, 21].

We consider the preparation of two independent 1D quasi-condensates. If they are prepared by cooling two independent quasi-condensates, the temperature of the left quasi-condensate T_{L} and that of the right quasi-condensate T_{R} are generically different. The density matrix of the initial state is described by $\hat{\rho}_0 = \mathrm{e}^{-(\beta_{\mathrm{L}} H_{\mathrm{L}} + \beta_{\mathrm{R}} H_{\mathrm{R}})}$, where $\beta_a = 1/(k_{\mathrm{B}} T_a)$ with $a = L, R$. It is important to note that the constant shift of phase $\phi_a \to \phi_a + \theta_{ac}$ does not change the energy of the system, so that for the average over thermal ensemble one has to integrate over θ_{ac}. Physically, this simply means that the phases of independent condensates are random. Then the only interesting distribution here is the distribution of the interference contrast [14, 18, 26, 68] given by

$$\hat{C}^2 = \left| \int_{-l/2}^{l/2} \mathrm{e}^{-\mathrm{i}\hat{\phi}_{\mathrm{s}}(r)} \right|^2 \mathrm{d}r, \tag{47}$$

which corresponds to, in spin language, the squared transverse magnitude of the spin $(\hat{S}_l^{\perp})^2$. The analysis of the evaluation of distributions in the density matrix of the thermal equilibrium state in section 5 can be directly extended to this case, and we obtain the distribution

$$P_l^{\perp}(\gamma) = \prod_k \int_{-\pi}^{\pi} \frac{\mathrm{d}\lambda_{\theta sk}}{2\pi} \int_0^{\infty} \lambda_{rsk}\, \mathrm{e}^{-\lambda_{rsk}^2/2}\, \mathrm{d}\lambda_{rsk}\, \delta\left(\gamma - \left| \rho \int_{-l/2}^{l/2} \mathrm{d}r\, \mathrm{e}^{\mathrm{i}\chi(r, \{\lambda_{jsk}\})} \right|^2 \right), \tag{48}$$

$$\begin{aligned} \chi(r, \{\lambda_{jsk}\}) &= \sum_k \sqrt{\frac{\langle |\hat{\phi}_{\mathrm{s},k}|^2 \rangle}{L}} \lambda_{rsk} \sin(kr + \lambda_{\theta sk}), \\ \langle |\hat{\phi}_{\mathrm{s},k}|^2 \rangle &= \frac{1 + \mathrm{e}^{-\beta_{\mathrm{L}}|k|c_{\mathrm{L}}}}{1 - \mathrm{e}^{-\beta_{\mathrm{L}}|k|c_{\mathrm{L}}}} \frac{\pi}{2|k|K_{\mathrm{L}}} + \frac{1 + \mathrm{e}^{-\beta_{\mathrm{R}}|k|c_{\mathrm{R}}}}{1 - \mathrm{e}^{-\beta_{\mathrm{R}}|k|c_{\mathrm{R}}}} \frac{\pi}{2|k|K_{\mathrm{R}}}, \end{aligned} \tag{49}$$

where c_a and K_a, $a = L, R$, are the sound velocity and Luttinger parameters of the left and right quasi-condensates.

6.3. Prethermalization of interference patterns

In section 2.3, we gave a heuristic argument for prethermalization phenomena, where the distributions of the interference contrast amplitudes of the two *non-equilibrium* quasi-condensates are given by that of two *equilibrium* quasi-condensates at some effective temperature T_{eff}. We identified the effective temperature to be the energy stored in each momentum mode. In section 4.2.5, we found this energy to be $\frac{\pi c_{\mathrm{s}} \rho \eta}{4K_{\mathrm{s}}}$; thus we conclude that $k_{\mathrm{B}} T_{\mathrm{eff}} = \frac{\pi c_{\mathrm{s}} \rho \eta}{4K_{\mathrm{s}}}$.

In the following, we formally derive the result above, using the expressions for full distributions of interference patterns. The distribution of the interference contrast is determined by $\langle |\hat{\phi}_{\mathrm{s},k}|^2 \rangle$ given in equation (20). In the long time limit, we can take $\sin^2(c_{\mathrm{s}}|k|t) \sim \cos^2(c_{\mathrm{s}}|k|t) \sim 1/2$. Moreover, since the interference contrast is most affected

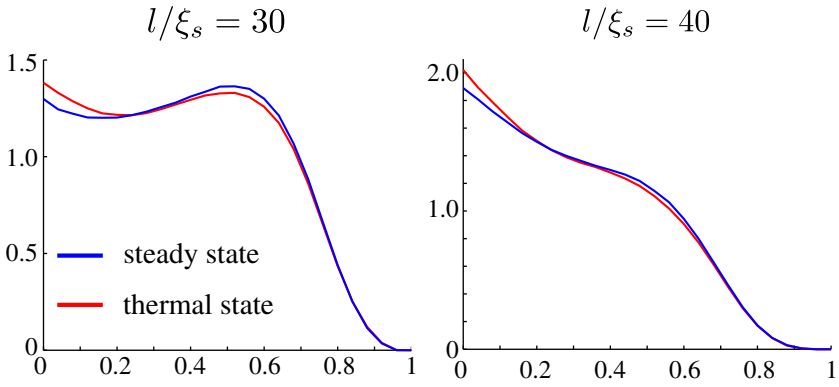

Figure 10. The distributions of interference contrast for steady states of split quasi-condensates and two thermal quasi-condensates. Here the x-axis is scaled such that the maximum value of interference contrast is 1. For the split condensates, we plot the distribution at time $t = 60\xi_s/c_s$ for the Luttinger parameter $K_s = 20$, system size $L = 400\xi_s$ and two different integration lengths $l/\xi_s = 30$ and 40. The thermal quasi-condensates are for temperature $\frac{\pi c_s}{2\xi_s}$ for the same integration length corresponding to the effective temperature obtained in equation (52).

by the excitations with small wave vectors k with $\alpha_k = \frac{|k|K_s}{\pi\rho\eta} < 1$, we can approximate the expression as

$$\langle|\hat{\phi}_{s,k}|^2\rangle \approx \frac{\pi}{2|k|K_s}\frac{\pi\rho\eta}{2|k|K_s}. \tag{50}$$

On the other hand, for two quasi-condensates in thermal equilibrium, the position of the interference peaks is again random. The interference contrast is determined by $\langle|\hat{\phi}_{s,k}|^2\rangle$ given in equation (49). Since the main contribution to the fluctuation comes from low momenta, we approximate $e^{-\beta|k|c} \approx 1 - \beta|k|c$. It is easy to check that the sound velocity and Luttinger parameters for each condensate are related to those of the difference mode (see equations (44)–(46)) as $c_L = c_R = c_s$ and $K_L = K_R = 2K_s$. Thus, we obtain

$$\langle|\hat{\phi}_{s,k}|^2\rangle \approx \frac{2}{\beta|k|c_s}\frac{\pi}{2|k|K_s}. \tag{51}$$

Now the crucial observation is that our closed form expressions for distributions of interference contrasts of both split quasi-condensates and thermal quasi-condensates are determined solely by $\langle|\hat{\phi}_{s,k}|^2\rangle$, and they take precisely the same form in terms of $\langle|\hat{\phi}_{s,k}|^2\rangle$. Moreover, the expressions given by equations (50) and (51) have the same dependence on wave vectors $|k|$. Therefore, the *full* distribution of interference contrast of split condensates becomes indistinguishable from that of thermal condensates with temperature

$$k_B T_{\text{eff}} \approx \frac{\pi c_s \rho\eta}{4K_s} = \frac{\mu\eta}{2}, \tag{52}$$

where the second equality holds for weakly interacting bosons and the chemical potential of one quasi-condesate is given by $\mu = g\rho$. Thus, split 1D quasi-condensates indeed display the prethermalization phenomenon.

In figure 10, we plot the interference contrast $P_l^{\perp}(\gamma)$ (see equation (25)) of split condensates in a steady state at time $t = 60\xi_s/c_s$ for the Luttinger parameter $K_s = 20$, the

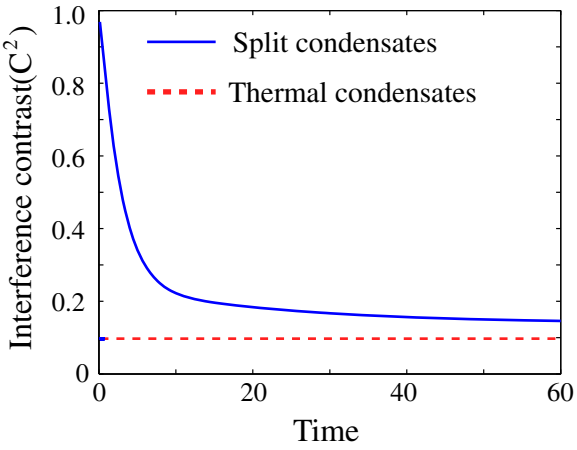

Figure 11. The evolution of the interference contrast $\hat{C}^2$ for the system size $L = 500\xi_s$, the integration length $l = 40\xi_s$ and the effective spin Luttinger parameter $K_s = 20$ with initial temperature corresponding to the chemical potential μ. Time is measured in units of ξ_s/c_s. Here we took the density $\rho_R = 1.2\rho$ and $\rho_L = 0.8\rho$. The magnitude of $\hat{C}^2$ for two thermal quasi-condensates at temperature $k_B T = \mu$ is plotted as a red dotted line for comparison.

system size $L = 400\xi_s$ and two different integration lengths $l/\xi_s = 30$ and 40. Also we plot the interference contrast of the thermal quasi-condensates (see equation (48)) at temperature $\frac{\pi c_s}{2\xi_s}$ for the same integration length. This temperature corresponds to the effective temperature obtained in equation (52). Indeed we see only a small difference between the distributions of steady states and thermal states for both integration lengths. The small difference comes from the approximations made in obtaining the expressions given by equations (50) and (51).

In previous paragraphs, we assumed that the splitting prepares quasi-condensates with identical average densities. Here, we briefly consider the case in which the splitting process prepares two quasi-condensates with slightly different densities. In this case, the temperature of the initial quasi-condensates affects the interference contrast around the time scale of $\frac{\xi_s}{(c_L - c_R)\pi} \approx \frac{\hbar}{\mu(\sqrt{\rho_L} - \sqrt{\rho_R})}$, whereas the prethermalized, long-time transient state is reached around $\frac{\hbar}{\mu}\frac{l}{\xi_s}$, where l is the integration length.

These analytic arguments can be confirmed through numerical simulations. In figure 11, we have plotted the evolution of the interference contrast $\hat{C}^2$ for the system size $L = 500\xi_s$, the integration length $l = 40\xi_s$ and the Luttinger parameter $K_s = 20$ with initial temperature corresponding to the chemical potential μ. Here we consider a situation where the density of the left quasi-condensate is different from that of the right quasi-condensate by 20% such that $\rho_R = 1.2\rho$ and $\rho_L = 0.8\rho$, where $\rho_{R(L)}$ is the average density of the right (left) condensate and 2ρ is the average density of the initial condensate before splitting. Also for comparison we have plotted the magnitude of interference contrast of two quasi-condensates in *thermal* states at a temperature given by μ. From the plot, one can observe the existence of quasi-steady state plateau after a short time. Note that the magnitude of $\hat{C}^2$ in the steady state is larger than the value expected from thermalized states at the initial temperature. The subsequent slow decrease of the interference contrast is due to the effect of temperature on the initial state coming from the small difference of the two quasi-condensates. Such a development of the plateaus at a larger

value of the interference contrast than that for the equilibrium state of the initial temperature indicates the phenomenon of prethermalization.

7. Conclusion

In this work, we have shown how the noise captured by full distribution functions can be used to study the dynamics of a many-body system in 1D. The analytical results for joint distribution functions obtained in section 4.2 allow not only the simple understanding of distribution functions from the spin-wave picture, but also an intuitive visualization of the correlation in a 1D system. Using this picture, we have also shown that the phenomenon of prethermalization occurs in 1D dynamics. The thermal-like behavior of the prethermalized state is revealed by using the full distribution functions that contain information about the correlation functions of arbitrary order. For an experimental demonstration of such prethermalizations, see [24].

The approach developed in this paper can be extended to other types of dynamics. While we focused on the Ramsey-type dynamics or dynamics of interference patterns for a split quasi-condensate, we can also change different physical parameters to induce the dynamics. For example, it is straightforward to apply our study to the sudden change (quench) of interaction strength [40, 70].

In this paper, we focused on distribution functions obtained from the Tomonaga–Luttinger Hamiltonian (4). It is of interest to extend our analysis to higher spins [71], and analyze them, for example, in the presence of a magnetic field [72]. Since there are more degrees of freedom in these systems, distributions might capture the tendency towards various phases such as ferromagnetic ordering. These questions will be analyzed in future work.

Acknowledgments

We thank Igor Mazets, Alexei Gorshkov and Susanne Pielawa for useful discussions. TK and ED acknowledge support from a grant from the Army Research Office and funding from the DARPA OLE program, Harvard–MIT CUA, NSF grant no. DMR-07-05472, AFOSR Quantum Simulation MURI and the ARO-MURI on atomtronics. AI acknowledges support from the Texas Norman Hackerman Advanced Research Program under grant no. 01889 and the NSF Career Award and JS is supported by the Austrian FWF through the Wittgenstein Prize.

Appendix A. Distribution function of the *z* component of spin

In this appendix, we calculate the distribution function of $\hat{S}_l^z$ in the absence of coupling between charge and spin. Extension to the case in which the charge and spin degrees of freedom mix is straightforward.

It is convenient to evaluate the generating function $\langle e^{\lambda \hat{S}_l^z} \rangle$, instead of distribution function $P_l^z(\alpha)$. They are related by

$$\langle e^{\lambda \hat{S}_l^z} \rangle = \int_{-\infty}^{\infty} e^{\lambda \alpha} P_l^z(\alpha)\, d\alpha. \tag{A.1}$$

This equality can be checked by differentiating both sides by λ and evaluating them at $\lambda = 0$. This reproduces the implicit definition of P_l^z in equation (2).

Analogous to the calculation of the mth moment of $\hat{S}_l^\theta$, we first express $\hat{S}_l^z$ in terms of $\gamma_{s,k}$ operators defined in equation (15)

$$\hat{S}_l^z(r) = \int_{-l/2}^{l/2} \mathrm{d}r \left(\sum_{k\neq 0} (d_{s,k}\gamma_{s,k}^\dagger + d_{s,k}^* \gamma_{s,-k}) \mathrm{e}^{\mathrm{i}kr} + \frac{n_{s,0}}{\sqrt{L}} \right),$$

$$d_{s,k} = \sqrt{\frac{|k|K_s}{2\pi L}} \frac{\mathrm{e}^{\mathrm{i}c_s|k|t} + 2W_k \mathrm{e}^{-\mathrm{i}c_s|k|t}}{\sqrt{1-4|W_k|^2}}.$$

Then, we can apply the trick introduced in section 4.2 to obtain

$$\langle \mathrm{e}^{\lambda \hat{S}_l^z} \rangle = \mathrm{e}^{\lambda^2 \int_{-l/2}^{l/2} \mathrm{d}r_1 \mathrm{d}r_2 (\sum_{k\neq 0} |d_{s,k}|^2 \mathrm{e}^{\mathrm{i}k(r_1-r_2)} + \frac{\langle n_{s,0}^2 \rangle}{\sqrt{L}})}$$

$$= \exp\left\{ \lambda^2 \left(\frac{\rho\eta l^2}{4L} + \sum_{k\neq 0} \frac{4|d_{s,k}|^2}{k^2} \sin^2(lk/2) \right) \right\}.$$

Then the following expression gives the distribution of $\hat{S}_l^z$:

$$P_l^z(\alpha) = \frac{1}{2\sqrt{\pi \langle (\hat{S}_l^z)^2 \rangle}} \exp\left(-\frac{\alpha^2}{4\langle (\hat{S}_l^z)^2 \rangle} \right), \tag{A.2}$$

where

$$\langle (\hat{S}_l^z)^2 \rangle = \frac{\rho\eta l^2}{4L} + \sum_{k\neq 0} \frac{4|d_{s,k}|^2}{k^2} \sin^2(lk/2).$$

Appendix B. Expression for $C_{a,k}$ in the presence of mixing between charge and spin

In this section, we derive the expression for $C_{a,k}$, $a = s, c$ in equation (36). We first find the transformation from $b_{s,k}$,$b_{c\uparrow,k}$ to $b_{1,k}, b_{2,k}$. Then we relate $b_{1,k}, b_{2,k}$ and $\gamma_{s,k}(t)$, $\gamma_{c,k}(t)$. Combining these two transformations, we obtain $b_{s,k}$ in terms of $\gamma_{s,k}(t)$, $\gamma_{c,k}(t)$, leading to the expression for $\hat{\phi}_{s,k}$ in terms of $\gamma_{s,k}(t)$, $\gamma_{c,k}(t)$.

From the relations

$$\phi_{i,k} = -\mathrm{i}\sqrt{\frac{\pi}{2|k|K_i}} (b_{i,k}^\dagger - b_{i,-k}),$$

$$n_{i,k} = \sqrt{\frac{|k|K_i}{2\pi}} (b_{i,k}^\dagger + b_{i,-k}),$$

$$b_{i,k}^\dagger = \mathrm{i}\phi_{i,k}\sqrt{\frac{|k|K_i}{2\pi}} + n_{i,k}\sqrt{\frac{\pi}{2|k|K_i}},$$

along with equation (29), it is straightforward to obtain

$$\begin{pmatrix} b^{\dagger}_{\mathrm{c}\uparrow,-k} \\ b_{\mathrm{c}\uparrow,k} \\ b^{\dagger}_{\mathrm{s},-k} \\ b_{\mathrm{s},k} \end{pmatrix} = D \begin{pmatrix} b^{\dagger}_{1,-k} \\ b_{1,k} \\ b^{\dagger}_{2,-k} \\ b_{2,k} \end{pmatrix},$$

where

$$D = \frac{1}{2}$$

$$\begin{pmatrix} \cos\kappa\left(\sqrt{\frac{\tilde{K}_{\mathrm{c}\uparrow}}{K_1}}+\sqrt{\frac{K_1}{\tilde{K}_{\mathrm{c}\uparrow}}}\right) & \cos\kappa\left(-\sqrt{\frac{\tilde{K}_{\mathrm{c}\uparrow}}{K_1}}+\sqrt{\frac{K_1}{\tilde{K}_{\mathrm{c}\uparrow}}}\right) & -\sin\kappa\left(\sqrt{\frac{\tilde{K}_{\mathrm{c}\uparrow}}{K_2}}+\sqrt{\frac{K_2}{\tilde{K}_{\mathrm{c}\uparrow}}}\right) & -\sin\kappa\left(-\sqrt{\frac{\tilde{K}_{\mathrm{c}\uparrow}}{K_2}}+\sqrt{\frac{K_2}{\tilde{K}_{\mathrm{c}\uparrow}}}\right) \\ \cos\kappa\left(-\sqrt{\frac{\tilde{K}_{\mathrm{c}\uparrow}}{K_1}}+\sqrt{\frac{K_1}{\tilde{K}_{\mathrm{c}\uparrow}}}\right) & \cos\kappa\left(\sqrt{\frac{\tilde{K}_{\mathrm{c}\uparrow}}{K_1}}+\sqrt{\frac{K_1}{\tilde{K}_{\mathrm{c}\uparrow}}}\right) & -\sin\kappa\left(-\sqrt{\frac{\tilde{K}_{\mathrm{c}\uparrow}}{K_2}}+\sqrt{\frac{K_2}{\tilde{K}_{\mathrm{c}\uparrow}}}\right) & -\sin\kappa\left(\sqrt{\frac{\tilde{K}_{\mathrm{c}\uparrow}}{K_2}}+\sqrt{\frac{K_2}{\tilde{K}_{\mathrm{c}\uparrow}}}\right) \\ \sin\kappa\left(\sqrt{\frac{K_{\mathrm{s}}}{K_1}}+\sqrt{\frac{K_1}{K_{\mathrm{s}}}}\right) & \sin\kappa\left(-\sqrt{\frac{K_{\mathrm{s}}}{K_1}}+\sqrt{\frac{K_1}{K_{\mathrm{s}}}}\right) & \cos\kappa\left(\sqrt{\frac{K_{\mathrm{s}}}{K_2}}+\sqrt{\frac{K_2}{K_{\mathrm{s}}}}\right) & \cos\kappa\left(-\sqrt{\frac{K_{\mathrm{s}}}{K_2}}+\sqrt{\frac{K_2}{K_{\mathrm{s}}}}\right) \\ \sin\kappa\left(-\sqrt{\frac{K_{\mathrm{s}}}{K_1}}+\sqrt{\frac{K_1}{K_{\mathrm{s}}}}\right) & \sin\kappa\left(\sqrt{\frac{K_{\mathrm{s}}}{K_1}}+\sqrt{\frac{K_1}{K_{\mathrm{s}}}}\right) & \cos\kappa\left(-\sqrt{\frac{K_{\mathrm{s}}}{K_2}}+\sqrt{\frac{K_2}{K_{\mathrm{s}}}}\right) & \cos\kappa\left(\sqrt{\frac{K_{\mathrm{s}}}{K_2}}+\sqrt{\frac{K_2}{K_{\mathrm{s}}}}\right) \end{pmatrix}, \tag{B.1}$$

where $\tilde{K}_{\mathrm{c}\uparrow} = K_{\mathrm{c}\uparrow}/\sqrt{s_{\mathrm{c}}}$.

Next, we relate $\gamma_{a,k}(t)$, $a = \mathrm{c}, \mathrm{s}$ operators to b_1, b_2. At $t = 0$, we have the relation between $\gamma_{a,k}(0)$, $a = \mathrm{c}, \mathrm{s}$ and $b_{\mathrm{c}\uparrow,k}$ and $b_{\mathrm{s},k}$ as described in section 5. Since operators $b_{\mathrm{c}\uparrow,k}$ and $b_{\mathrm{s},k}$ are related to $b_{1,k}$ and $b_{2,k}$ through the matrix D in equation (B.1), we can express $\gamma_{a,k}(0)$ as a linear combination of $b_{1,k}$ and $b_{2,k}$. The time evolution of $\gamma_{a,k}(0)$ is quite simple now, because Hamiltonians are diagonal in the bases $b_{1,k}$ and $b_{2,k}$. These considerations lead to the relations

$$\begin{pmatrix} \gamma^{\dagger}_{\mathrm{c},-k}(t) \\ \gamma_{\mathrm{c},k}(t) \\ \gamma^{\dagger}_{\mathrm{s},-k}(t) \\ \gamma_{\mathrm{s},k}(t) \end{pmatrix} = E_k \begin{pmatrix} \mathrm{e}^{-\mathrm{i}c_1|k|t} b^{\dagger}_{1,-k} \\ \mathrm{e}^{\mathrm{i}c_1|k|t} b_{1,k} \\ \mathrm{e}^{-\mathrm{i}c_2|k|t} b^{\dagger}_{2,-k} \\ \mathrm{e}^{\mathrm{i}c_2|k|t} b_{2,k} \end{pmatrix},$$

$$E_k = F_k D,$$

$$F_k = \begin{pmatrix} 1 & 0 & 0 & 0 \\ 0 & 1 & 0 & 0 \\ 0 & 0 & \dfrac{1}{\sqrt{1-4|W_k|^2}} & \dfrac{-2W_k}{\sqrt{1-4|W_k|^2}} \\ 0 & 0 & \dfrac{-2W_k}{\sqrt{1-4|W_k|^2}} & \dfrac{1}{\sqrt{1-4|W_k|^2}} \end{pmatrix}.$$

Now define a matrix $G(k) = DE_k^{-1}$ so that

$$\begin{pmatrix} b^\dagger_{\mathrm{c},-k} \\ b_{\mathrm{c},k} \\ b^\dagger_{\mathrm{s},-k} \\ b_{\mathrm{s},k} \end{pmatrix} = G(k) \begin{pmatrix} \gamma^\dagger_{\mathrm{c},-k} \\ \gamma_{\mathrm{c},k} \\ \gamma^\dagger_{\mathrm{s},-k} \\ \gamma_{\mathrm{s},k} \end{pmatrix}.$$

Then, finally, $C_{i,k}$ are given by

$$\begin{aligned} C_{\mathrm{s},k} &= -\mathrm{i}\sqrt{\frac{\pi}{2L|k|K_\mathrm{s}}}(G_{34}(k) - G_{44}(k)), \\ C_{\mathrm{c},k} &= -\mathrm{i}\sqrt{\frac{\pi}{2L|k|K_\mathrm{s}}}(G_{32}(k) - G_{42}(k)), \end{aligned} \tag{B.2}$$

where $G_{ij}(k)$ are the matrix elements of $G(k)$.

Appendix C. The $k = 0$ contribution in the presence of mixing between charge and spin

In this appendix, we evaluate $\mathrm{Tr}\{\mathrm{e}^{\mathrm{i}(\sum_i s_i)\phi_{s,0}/\sqrt{L}}\rho(t)\}$.

We first obtain the operator $\mathrm{e}^{\mathrm{i}(\sum_i s_i)\phi_{s,0}}$ after time evolution as

$$\mathrm{e}^{\mathrm{i}Ht}\mathrm{e}^{\mathrm{i}(\sum_i s_i)\phi_{s,0}}\,\mathrm{e}^{-\mathrm{i}Ht} = \exp\left(\mathrm{i}\frac{\sum_i s_i}{\sqrt{L}}(A\phi_{\mathrm{s},0} + A' n_{\mathrm{s},0} + \frac{B}{\sqrt{s_\mathrm{c}}}\phi_{\mathrm{c},0} + \frac{B'}{\sqrt{s_\mathrm{c}}} n_{\mathrm{c},0})\right). \tag{C.1}$$

The coefficients A, A', B and B' can be found as follows. The $k = 0$ part of the Hamiltonian is given by $H_0 = \frac{\pi c_1}{2K_1} n_{1,0}^2 + \frac{\pi c_2}{2K_2} n_{2,0}^2$ (see equation (11)). Using the commutation relation $[n_{i,0}, \phi_{i,0}] = -\mathrm{i}$, we have $\mathrm{e}^{\mathrm{i}Ht}\phi_{i,0}\,\mathrm{e}^{-\mathrm{i}Ht} = \phi_{i,0} + \frac{\pi c_i}{K_i} n_{i,0} t$. With the relation $\phi_{\mathrm{s},0} = \sin\kappa\,\phi_{1,0} + \cos\kappa\,\phi_{2,0}$, we obtain

$$\mathrm{e}^{\mathrm{i}Ht}\,\mathrm{e}^{(\sum_i s_i)\phi_{\mathrm{s},0}}\,\mathrm{e}^{-\mathrm{i}Ht} = \mathrm{e}^{\mathrm{i}\frac{\sum_i s_i}{\sqrt{L}}\left\{\sin\kappa(\phi_{1,0} + \frac{\pi c_1}{K_1} n_{1,0} t) + \cos\kappa(\phi_{2,0} + \frac{\pi c_2}{K_2} n_{2,0} t)\right\}}.$$

Now by transforming back to c, s bases through equation (29), we find

$$\begin{aligned} A &= 1, \\ A' &= \sin^2\kappa\,\frac{\pi c_1}{K_1} t + \cos^2\kappa\,\frac{\pi c_2}{K_2} t, \\ B &= 0, \\ B' &= \sin\kappa\cos\kappa\left(\frac{\pi c_1}{K_1} - \frac{\pi c_2}{K_2}\right) t. \end{aligned}$$

Now that we know the operator after time evolution equation (C.1), we evaluate it in the initial state.

The initial state of the spin sector is $|\psi_{s,k=0}\rangle$ in equation (12). Since this state is Gaussian, we have the simple result given below:

$$\langle\psi_{s,k=0}|\exp\left(\left(\sum_i s_i\right)(A\phi_{s,0}+A'n_{s,0})/\sqrt{L}\right)|\psi_{s,k=0}\rangle,$$
$$=\exp\left(-\left(\sum_i s_i\right)^2\left(\frac{1}{4\rho\eta L}+(A')^2\frac{\rho\eta}{4L}\right)\right).$$

For the charge sector, the $k=0$ part of the initial density matrix is $\frac{1}{\mathcal{N}_{c0}}\exp(-\beta\frac{\pi c_{c\uparrow}}{2K_{c\uparrow}}n_{c,0}^2)$, where $\mathcal{N}_{c0}$ is the normalization $\mathcal{N}_{c0}=\mathrm{Tr}(\exp(-\beta\frac{\pi c_{c\uparrow}}{2K_{c\uparrow}}n_{c,0}^2))$. The evaluation of the charge sector yields

$$\frac{1}{\mathcal{N}_{c0}}\mathrm{Tr}\left\{\exp\left(\mathrm{i}\left(\sum_i s_i\right)B'\frac{n_{c,0}}{\sqrt{s_c L}}\right)\exp\left(-\beta\frac{\pi c_{c\uparrow}}{2K_{c\uparrow}}n_{c,0}^2\right)\right\}=\exp\left(-\left(\sum_i s_i\right)^2(B')^2\frac{\tilde{K}_{c\uparrow}}{2\pi c_{c\uparrow}\beta L}\right).$$

Collecting the results above, we conclude that

$$\langle e^{\mathrm{i}(\sum_i s_i)\phi_{s,0}/\sqrt{L}}\rangle=\exp\left(-\frac{\left(\sum_i s_i\right)^2}{4L}\left\{\frac{1}{\rho\eta}+\rho\eta(A')^2+(B')^2\frac{2\tilde{K}_{c\uparrow}}{\pi c_{c\uparrow}\beta}\right\}\right).$$

References

[1] Aspect A, Grangier P and Roger G 1982 *Phys. Rev. Lett.* **49** 91
[2] Kindermann M 2007 *Nature* **448** 262
[3] Saminadayar L, Glattli D, Jin Y and Etienne B 1997 *Phys. Rev. Lett.* **79** 2526
[4] De-Picciotto R *et al* 1997 *Nature* **389** 162
[5] Dolev M, Heiblum M, Umansky V, Stern A and Mahalu D 2008 *Nature* **452** 829
[6] Öttl A, Ritter S, Köhl M and Esslinger T 2005 *Phys. Rev. Lett.* **95** 090404
[7] Aspect A, Boiron D and Westbrook C 2008 *Europhys. News* **39** 25
[8] Hadzibabic Z, Stock S, Battelier B, Bretin V and Dalibard J 2004 *Phys. Rev. Lett.* **93** 180403
[9] Spielman I, Phillips W and Porto J 2007 *Phys. Rev. Lett.* **98** 080404
[10] Guarrera V *et al* 2008 *Phys. Rev. Lett.* **100** 250403
[11] Fölling S *et al* 2005 *Nature* **434** 481
[12] Rom T *et al* 2006 *Nature* **444** 733
[13] Greiner M, Regal C A, Stewart J T and Jin D S 2005 *Phys. Rev. Lett.* **94** 110401
[14] Hofferberth S *et al* 2008 *Nat. Phys.* **4** 489
[15] Chabanov V and Zakhariev B 2001 *Phys. Rev. Lett.* **87** 160408
[16] Richard S *et al* 2003 *Phys. Rev. Lett.* **91** 010405
[17] Imambekov A *et al* 2009 *Phys. Rev.* A **80** 033604
[18] Imambekov A, Gritsev V and Demler E 2008 *Phys. Rev.* A **77** 063606
[19] Hadzibabic Z, Krüger P, Cheneau M, Battelier B and Dalibard J 2006 *Nature* **441** 1118
[20] Manz S *et al* 2010 *Phys. Rev.* A **81** 031610
[21] Betz T *et al* 2011 *Phys. Rev. Lett.* **106** 020407
[22] Widera A *et al* 2008 *Phys. Rev. Lett.* **100** 140401

[23] Hofferberth S, Lesanovsky I, Fischer B, Schumm T and Schmiedmayer J 2007 *Nature* **449** 324
[24] Gring M *et al* unpublished work
[25] Imambekov A, Gritsev V and Demler E 2007 *Proc. Enrico Fermi Summer School on Ultracold Fermi Gases 2006* (Amsterdam: IOS Press) (arXiv:cond-mat/0703766v1)
[26] Polkovnikov A, Altman E and Demler E 2006 *Proc. Natl Acad. Sci. USA* **103** 6125
[27] Lamacraft A and Fendley P 2008 *Phys. Rev. Lett.* **100** 165706
[28] Caux J-S and Calabrese P 2006 *Phys. Rev.* A **74** 031605
[29] Imambekov A and Glazman L I 2008 *Phys. Rev. Lett.* **100** 206805
[30] Gangardt D and Shlyapnikov G 2003 *Phys. Rev. Lett.* **90** 010401
[31] Lieb E H and Liniger W 1963 *Phy. Rev.* **130** 1605
[32] Frahm H and Palacios G 2005 *Phys. Rev.* A **72** 061604(R)
[33] Batchelor M T, Bortz M, Guan X W and Oelkers N 2005 *Phys. Rev.* A **72** 061604
[34] Imambekov A and Demler E 2006 *Ann. Phys.* **321** 2390
[35] Imambekov A and Demler E 2006 *Phys. Rev.* A **73** 021602
[36] Orso G 2007 *Phys. Rev. Lett.* **98** 070402
[37] Tokatly I V 2004 *Phys. Rev. Lett.* **93** 090405
[38] Fuchs J N, Recati A and Zwerger W 2004 *Phys. Rev. Lett.* **93** 090408
[39] Lieb E H 1963 *Phys. Rev.* **130** 1616
[40] Cazalilla M A 2006 *Phys. Rev. Lett.* **97** 156403
Iucci A and Cazalilla M A 2010 *New J. Phys.* **12** 055019
[41] Giamarchi T 2004 *Quantum Physics in One Dimension* (*International Series of Monographs on Physics*) (New York: Oxford University Press)
[42] Cazalilla M A, Citro R, Giamarchi T, Orignac E and Rigol M 2011 arXiv:1101.5337
[43] Gritsev V, Demler E, Lukin M and Polkovnikov A 2007 *Phys. Rev. Lett.* **99** 200404
[44] De Grandi C, Barankov R and Polkovnikov A 2008 *Phys. Rev. Lett.* **101** 230402
[45] Barmettler P, Punk M, Gritsev V, Demler E and Altman E 2009 *Phys. Rev. Lett.* **102** 130603
[46] Schollwöck U 2005 *Rev. Mod. Phys.* **77** 259
[47] Kinoshita T, Wenger T and Weiss D S 2006 *Nature* **440** 900
[48] Rigol M, Dunjko V and Olshanii M 2008 *Nature* **452** 854
[49] Cassidy A, Mason D, Dunjko V and Olshanii M 2009 *Phys. Rev. Lett.* **102** 025302
[50] Wineland D, Bollinger J, Itano W and Heinzen D 1994 *Phys. Rev.* A **50** 67
[51] Sørensen A, Duan L M, Cirac J I and Zoller P 2001 *Nature* **409** 63
[52] Kitagawa T *et al* 2010 *Phys. Rev. Lett.* **104** 255302
[53] Folman R *et al* 2000 *Phys. Rev. Lett.* **84** 4749
[54] Reichel J and Vuletic V (ed) 2011 *Atom Chips* (New York: Wiley)
[55] Bederson B 2002 *Adv. At. Mol. Opt. Phys.* **48** 263
[56] Wicke P, Whitlock S and van Druten N J 2010 arXiv:1010.4545v1
[57] Schumm T *et al* 2005 *Nat. Phys.* **1** 57
[58] Berges J, Borsányi S and Wetterich C 2004 *Phys. Rev. Lett.* **93** 142002
[59] Barnett R, Polkovnikov A and Vengalattore M 2010 arXiv:1009.1646v2
[60] Mathey L and Polkovnikov A 2010 *Phys. Rev.* A **81** 033605
[61] Mazets I E, Schumm T and Schmiedmayer J 2008 *Phys. Rev. Lett.* **100** 210403
[62] Mazets I E and Schmiedmayer J 2010 *New J. Phys.* **12** 055023
[63] Tan S, Pustilnik M and Glazman L I 2010 *Phys. Rev. Lett.* **105** 090404
[64] Burkov A A, Lukin M D and Demler E 2007 *Phys. Rev. Lett.* **98** 200404
Pereira R G, Sirker J, Caux J-S, Hagemans R, Maillet J M, White S R and Affleck I 2008 *Phys. Rev. Lett.* **100** 027206
Pustilnik M, Khodas M, Kamenev A and Glazman L I 2006 *Phys. Rev. Lett.* **96** 196405
Imambekov A and Glazman L I 2009 *Science* **323** 228
Imambekov A and Glazman L I 2009 *Phys. Rev. Lett.* **102** 126405

[65] Hadzibabic Z and Dalibard J 2011 *Riv. Nuovo Cimento* **34** 389–434
[66] Olshanii M 1998 *Phys. Rev. Lett.* **81** 938
[67] Bistritzer R and Altman E 2007 *Proc. Natl Acad. Sci. USA* **104** 9955
[68] Gritsev V, Altman E, Demler E and Polkovnikov A 2006 *Nat. Phys.* **2** 705
[69] Stimming H-P, Mauser N, Schmiedmayer J and Mazets I 2010 *Phys. Rev. Lett.* **105** 015301
[70] Iucci A and Cazalilla M A 2009 *Phys. Rev.* A **80** 063619
[71] Barnett R, Podolsky D and Refael G 2009 *Phys. Rev.* B **80** 024420
[72] Vengalattore M, Leslie S R, Guzman J and Stamper-Kurn D M 2008 *Phys. Rev. Lett.* **100** 170403